1	The macaque brain ONPRC18 template with combined gray and white matter
2 3	labelmap for multimodal neuroimaging studies of nonhuman primates
5 4 5	Abbreviated Title: The ONPRC18 multi-modal atlas for macaque brain
5 6 7 8	Alison R Weiss <sup>1</sup> , Zheng Liu <sup>1,2</sup> , Xiaojie Wang <sup>1,2</sup> , William A Liguore <sup>1</sup> , Christopher D. Kroenke <sup>1,2,3</sup> and Jodi L. McBride <sup>1,3,4*</sup>
9 10 11 12 13 14	1) Division of Neuroscience, Oregon National Primate Research Center, Beaverton, OR, USA, 97006; 2) Advanced Imaging Research Center, Oregon Health and Science University, Portland, OR, USA, 97239; 3) Departments of Behavioral Neuroscience and 4) Neurology, Oregon Health and Science University, Portland OR, USA, 97239
15	Corresponding author:
16	Jodi L. McBride, PhD* Associate Professor
17 18	Division of Neuroscience, Oregon National Primate Research Center
19	Department of Behavioral Neuroscience, Oregon Health and Science University
20	505 NW 185 <sup>th</sup> Avenue
21	Beaverton, OR 97006
22	USA
23	Office: (503) 346-5454
24	Fax: (503) 346-5513
25	Email: <u>mcbridej@ohsu.edu</u>
26	
27	
28	
29	
30	
31	

### 32 **ABSTRACT:**

33 Macagues are the most common nonhuman primate (NHP) species used in 34 neuroscience research. With the advancement of many neuroimaging techniques, new studies are beginning to apply multiple types of in vivo magnetic resonance imaging (MRI), such as 35 36 structural imaging (sMRI) with T1 and T2 weighted contrasts alongside diffusion weighed (DW) 37 imaging. In studies involving rhesus macaques, this approach can be used to better understand 38 micro-structural changes that occur during development, in various disease states or with 39 normative aging. However, many of the available rhesus brain atlases have been designed for 40 only one imaging modality, making it difficult to consistently define the same brain regions 41 across multiple imaging modalities in the same subject. To address this, we created a brain atlas 42 from 18 adult rhesus macaques that includes co-registered templates constructed from images 43 frequently used to characterize macroscopic brain structure (T2/SPACE and T1/MP-RAGE), and 44 a diffusion tensor imaging (DTI) template. The DTI template was up-sampled from 1 mm 45 isotropic resolution to resolution match to the T1 and T2-weighted images (0.5 mm isotropic). 46 and the parameter map was derived for fractional anisotropy (FA). The labelmap volumes 47 delineate 57 gray matter regions of interest (ROIs; 36 cortical regions and 21 subcortical 48 structures), as well as 74 white matter tracts. Importantly, the labelmap overlays both the 49 structural and diffusion templates, enabling the same regions to be consistently identified 50 across imaging modalities. A specialized condensed version of the labelmap ROIs are also 51 included to further extend the usefulness of this tool for imaging data with lower spatial 52 resolution, such as functional MRI (fMRI) or positron emission tomography (PET).

53

54 *Keywords:* macaque, brain atlas, DTI, MRI, cortico-basal ganglia networks

### 56 1 INTRODUCTION

57

58 Nonhuman primates (NHPs) are valuable for translational neuroscience due to their 59 relatively large and complex brain structure, their diverse behavioral repertoire, and their close 60 phylogenic relationship with humans. Many neuroimaging studies with macagues require a 61 species-specific magnetic resonance imaging (MRI) atlas to accurately delineate the anatomical 62 boundaries of brain regions. Recent advances in neuroimaging techniques have spurred the 63 generation of several NHP-specific MRI atlases and labelmaps, for example a T1-weighted MRI 64 template by Rohlfing et al. (2012), a T2-weighted MRI template by Calabrese et al. (2015), and 65 diffusion tensor imaging (DTI) templates by Zakszewski et al. (2014) and Adluru et al. (2012). Historically, atlases that have been designed for only one imaging modality represent a 66 challenge for studies employing multiple neuroimaging modalities in the same study 67 68 population. For such multi-modal neuroimaging studies, different templates can be applied 69 separately to each scan modality. However, a limitation to this approach is that the 70 corresponding label maps from each template may have slight-to-significant differences in 71 boundary definitions, making it difficult to consistently define the same brain regions across 72 multiple imaging modalities in the same subject.

To address this gap, we created a series of co-registered templates, including T1- and T2-weighted MRI as well as DTI. Regions of Interest (ROI) were defined to facilitate the investigation of cortico- and thalamo-basal ganglia circuitry and were informed by the boundaries described by Saleem & Logothetis (2007). This atlas builds on previous work from our group (Rohlfing et al., 2012) using non-linear spatial normalization techniques (Avants et al., 2008; Yeo et al., 2008) to generate rhesus brain templates, and integrates high-resolution images from multiple image contrasts.

80 We have also made practical improvements in the labelmap to facilitate multi-modal 81 neuroimaging studies. The INIA19 atlas (Rohlfing et al., 2012) applied NeuroMaps labels that 82 were originally defined on a histological dataset (BrainInfo, 1991-present). However, in 83 practice, we have found that both scan quality and individual variability in neuroanatomy 84 impact the reliability and accuracy of registration-based segmentation approaches using highly-85 detailed and complex labelmaps with small ROIs. Here, we created a labelmap with fewer, 86 more simplified ROIs that are better matched to the image resolution of in vivo MRI and more 87 tolerant of individual variation. To facilitate use of these templates for multimodal 88 neuroimaging studies, the T1-weighted, T2-weighted, and diffusion-based images are 89 registered to a common reference frame and labelmap. Moreover, to extend the usefulness of 90 this tool for imaging data with lower spatial resolution, such as positron emission tomography 91 (PET) or functional MRI (fMRI), a specialized condensed version of the labelmap ROIs was also 92 generated.

93

### 95 2 MATERIALS AND METHODS

96

### 97 2.1 Subjects

Eighteen male (n=6) and female (n=12) adult rhesus macaques (ages 5-12) contributed to this study (**Table 1**). At the time the scans were collected, the animals were pair housed in standard indoor caging, maintained on a 7am/7pm light/dark cycle, given ad libitum access to water, and provided with monkey chow rations and fresh produce daily. The Institutional Animal Care and Use Committee (IACUC) approved all procedures used in this study, and all of the guidelines specified in the National Institutes of Health Guide for the Care and Use of Laboratory Animals were strictly followed.

105 To prevent motion artifacts and to ensure the safety of the animals, all monkeys were 106 anesthetized for the duration of the scanning session. Anesthesia was initially induced with 107 Ketamine HCl (15mg/kg IM) and the animals were subsequently intubated to allow for maintenance of anesthesia by inhalation of 1-2% isoflurane gas vaporized in 100% oxygen. 108 109 Animals were then placed in a head first, supine position on the scanner bed, and their heads 110 were immobilized in the head coil with foam padding. Heart rate and blood oxygenation levels 111 were observed and recorded by trained veterinary staff throughout the duration of the 112 procedure. Upon completion of the scans, the animals were extubated, returned to their housing environment, and their recovery monitored closely for several hours. 113

114

### 115 **2.2 MRI acquisition procedures**

Images were acquired with a Siemens Prisma whole body 3T MRI system (Erlangen, Germany) using a 16-channel pediatric head rf coil. A vitamin E tablet taped to the right side of the head served as a fiducial marker. The images acquired included 3D T1-weighted

weighted sampling perfection with application optimized contrasts using differe evolution (SPACE) (Mugler et al., 2000), and diffusion tensor imaging (DTI). Detailed	n, 1990), 3D T2-
evolution (SPACE) (Mugler et al., 2000), and diffusion tensor imaging (DTI). Detailed	erent flip angle
	led parameters
122 for each scanning sequence are described in the sections that follow.	

123

124 2.2.1 T1-weighted MP-RAGE

- For 3D MP-RAGE imaging sequences, TE/TR/TI = 3.44/2600/913 ms, flip angle = 8°, voxel sizes were 0.5 mm isotropic and 224 slices were acquired. In-plane image sampling consisted of 320 by 320 data points in the phase-encoded and readout directions, respectively. Three MP-RAGE images were acquired in each imaging session and these were rigid-body registered to
- 129 each other and averaged. Total MP-RAGE acquisition time was 31 minutes and 9 seconds.

130

131 2.2.2 T2-weighted SPACE

For 3D SPACE imaging sequences, TE/TR = 385/3200 ms, flip angle = 120°, voxel sizes and the field of view were the same as the 3D MP-RAGE images described above. Three SPACE images were acquired in each imaging session and these were rigid-body registered to each other and averaged. Total SPACE acquisition time was 29 minutes and 42 seconds.

136

### 137 2.2.3 Diffusion Tensor Imaging

Diffusion-weighted volumes were acquired using a monopoplar 2D diffusion-weighted, spin-echo echo planar imaging (EPI) sequence (TR/TE = 6700 ms/73 ms, GRAPPA factor = 2, echo train length = 52, resolution =  $1 \times 1 \times 1$ mm). Seven repetitions of 6 b0 volumes and 30 DW volumes with single b =  $1000 \text{ s/mm}^2$  were acquired with the phase-encoding direction being anterior to posterior (A -> P). To correct for the susceptibility induced distortions inherent to

143 the EPI sequence, 1 b0 volume with opposite (P -> A) phase encoding directions was also

144 acquired. Total diffusion MRI acquisition time was 29 minutes and 39 seconds.

145

### 146 **2.3 MR image preprocessing**

A set of preprocessing operations was first applied to all acquired MR images to correct various types of artifacts and to extract brain masks. For T1-weighted and T2-weighted anatomic images (MP-RAGE and SPACE images), the artifacts, such as motion and intensity inhomogeneity, were corrected first, and then the brains were extracted for template construction. For DTI, the distortion of phase-encoding, motion and eddy current artifacts were corrected first, and subsequently the templates were constructed.

153

### 154 2.3.1 T1-weighted and T2-weighted anatomic image preprocessing

155 Both T1-weighted and T2-weighted images were preprocessed with identical procedures. In each imaging session, each of the three images were averaged after motion 156 157 correction. For the motion correction, the first scanned image in each modality was selected as 158 the reference, and other two images were registered to the reference using the rigid-body 159 transformation. Next, the registered images and the reference image were averaged. All 160 registration processing and averaging operations were carried out using ANTS (version 2.1; 161 http://stnava.github.io/ANTs/) and FSL (version 5.0, http://fsl.fmrib.ox.ac.uk/fsl/fslwiki/). For all 162 merged T1-weighed and T2-weighted images, intensity bias correction was performed using the 163 "N4BiasFieldCorrection" tool in ANTS (Tustison et al., 2010). Next, T1- and T2-weighted head 164 templates were constructed in the native coordinate using the "buildtemplateparallel.sh" tool 165 in ANTS (Avants et al., 2010). Brain masks were drawn manually for head templates, and all bias field corrected subject T1- and T2-weighted images were nonlinearly registered to the 166

167 corresponding head templates. With the resulting registration parameters, the template brain 168 masks were inversely mapped to each subject T1- and T2-weighted image spaces and the brains 169 were extracted by the brain mask. The process of intensity bias correction for all brain images 170 was repeated using the "N4BiasFieldCorrection" tool, in which the subject brain mask was used 171 to limit the correction region to improve correction quality.

172

### 173 2.3.2 DTI preprocessing

174 All the DW volumes first underwent a de-noising step implemented in MATLAB (using a 175 MATLAB script kindly provided by Dr. Sune Jespersen, Aarhus University) (Veraart et al., 2016). 176 Next, a susceptibility-induced off-resonance field (h) was calculated from the 6 pairs of b0 177 volumes with opposite phase-encoding direction using "topup," included in the FSL library 178 (https://fsl.fmrib.ox.ac.uk/) (Andersson et al., 2003). An eddy current induced off-resonance 179 field (e) and rigid-body transformations (r) between DW volumes to account for motion were 180 estimated simultaneously using "eddy" (FSL). Finally, the 3 transformations (h, e, and r) were 181 combined into one warp field to correct the de-noised DW volumes (Andersson and 182 Sotiropoulos, 2016). "DTIFIT", another tool included in FSL library, was used to fit the de-noised, 183 corrected bOs and DW volumes to a single tensor (DTI) model.

184

### 185 **2.4 Multi-modal template construction and atlas creation**

After preprocessing operations for the anatomic and DTI data were completed, population-based average brain templates were constructed. The T2-weighted template was constructed first as the reference for the other template constructions as described below.

- 189
- 190

### 191 2.4.1 T2-weighted template construction

192 All corrected T2-weighted brain images were initially aligned into a common space using 193 a previously published T2 template (Calabrese et al., 2015) by rigid-body registration with the 194 "antsRegistrationSyN.sh" tool. This reference frame was selected due to its high resolution and 195 excellent tissue contrast, as well its orientation in the standard 'MNI' space (Frey et al., 2011). 196 This way, all transformed brain images were represented in a commonly used reference frame, 197 possessing the same orientation and position. Next, an 'initial template' was generated from 198 the resulting images the "buildtemplateparallel.sh" using tool 199 (https://github.com/ANTsX/ANTs/blob/master/Scripts/buildtemplateparallel.sh) with one 200 iteration and affine registration, using the default similarity metric (probability mapping). Then, 201 the newly generated 'initial template' was used as the target and the template building 202 command was re-run in four iterations using fully deformable registrations. The output was the 203 final T2-weighted template.

204

### 205 2.4.2 T1-weighted template construction

206 The T2-weighted template was used as the reference for T1-weighted template 207 construction. First, each corrected T1-weighted brain image was aligned to the corresponding 208 T2-weighted brain image with a 12-parameter affine linear registration using mutual 209 information as a cost function with the "antsRegistrantionSyN.sh" tool. Next, all T2-weighted 210 brain images were b-spline non-linearly registered to the reference using the same software 211 (ANTS version 2.1; http://stnava.github.io/ANTs/) . Subsequently, with the resulting 212 parameters, all aligned T1-weighted brain images were transformed to the T2-weighted brain 213 template space. After averaging all transformed images, the T1-weighted brain template was 214 obtained, which resided in the same reference frame as the T2-weighted template.

215

### 216 2.4.4 DTI Template

217 The diffusion tensor template was constructed from all 18 individuals and resampled 218 with 0.5 mm isotropic voxel spacing using DTI-TK (https://www.nitrc.org/projects/dtitk), a 219 tensor-based spatial normalization tool (Zhang et al., 2007). The procedure described in Adluru 220 et al. (2012) was followed, in which tensor-based registrations were performed to generate a 221 diffusion MRI template, which was subsequently registered to the T2-weighted template. It has 222 been demonstrated that templates created using tensor-based methods (i.e. DTI-TK) perform 223 better than templates created using multimodal intrasubject registration methods (i.e. FA-T1 224 and BO-T2) (Adluru et al., 2012). For this reason, we adopted DTI-TK methods to generate the 225 DTI template and then aligned the DTI template to the anatomical template space where 226 multimodal registration operations were implemented only once, rather than to use 227 intrasubject registrations to bring each subject's DTI images into the space of the T2 before 228 template construction. Once completed, the diffusion tensor template was non-linearly 229 mapped to the T2-weighted template. To achieve this, the b0 template was first non-linearly 230 registered to the T2w template using "antsRegistrationSyn.sh", resulting in an affine transform 231 and a warp field. Next, the diffusion tensor template was warped to the T2w space using the 232 field generated from the affine transform and the warp previous step via 233 "antsApplyTransforms" (with -e 2 option). Lastly, the affine transform and the warp field were 234 combined into a single warp file which was used to reorient the diffusion tensors that were 235 already in T2-weighted template space. The DTI-TK TV tool was then used to generate tensor 236 derivatives (i.e. FA, MD, RD, and RGB color-coded FA images), which were subsequently 237 reoriented with ITK-SNAP into RPI orientation to match the T1 and T2 templates.

238

### 239 2.5 Gray Matter(GM) Labelmap

240 The atlas of Saleem & Logothetis (2007) was used to define the boundaries of all cortical 241 and subcortical Regions of Interest (ROIs) in the labelmap. ROIs were manually drawn on 242 coronal sections of the T2 template by trained neuroanatomical experts (A.R.W., W.A.L., J.L.M.), 243 using the 3D segmentation software ITK-SNAP (Yushkevich et al., 2006), and subsequently 244 verified and edited in the axial and sagittal planes. Table 2 describes the anatomical boundaries 245 used to delineate this labelmap, and **Figure 1A** provides 3-dimensional renderings of the ROIs. 246 Additionally, to facilitate neuroimaging modalities where scans have lower spatial resolution. 247 we created an auxiliary version of the GM labelmap with condensed cortical and sub-cortical ROIs (Table 2, Figure 1B). 248

249

### 250 2.6 Combined GM/WM labelmap

251 To provide segmentations of white matter (WM), we used a published diffusion tensor-252 based rhesus macaque atlas (Zakszewski et al., 2014) to identify and segment WM tracts on our 253 templates. In order to combine these WM ROIs with our gray-matter (GM) ROIs into one 254 consolidated labelmap, the WM labelmap was first applied to the FA template. To accomplish 255 this, the FA templaate from Zakszewski et al. (2014) was nonlinearly registered to our FA 256 template, and the resulting transformation applied to the WM labelmap. This process resulted in a number of voxels being redundantly labeled as GM and WM structures. Using ITK-snap, the 257 258 overlapping voxels were manually categorized by a trained observer (A.R.W.), and then 259 labelmaps combined using FSL commands. The cerebellum was defined in this atlas using only 260 one consolidated ROI and so all overlapping WM ROIs in this region were assigned to part of the 261 cerebellar ROI.

262

### 263 **3 RESULTS**

264

We created a series of co-registered templates, including T1- and T2-weighted MRI as well as DTI, that are aligned with a set of labelmaps that define Regions of Interest (ROI) to facilitate the investigation of cortico- and thalamo-basal ganglia circuitry.

268

### 269 **3.1 T1 and T2 templates and labelmaps**

270 The anatomical T1 and T2 templates have identical native resolution (0.5 mm isotropic), 271 and fields of view (60 mm by 79.5 mm by 50 mm). The templates are provided in neuroimaging 272 informatics technology initiative (NIFTI) file format with all associated meta-data formatted to 273 Brain Imaging Data Structure (BIDS) specifications (https://bids-274 specification.readthedocs.io/en/stable/), and have been submitted to the NITRC data exchange 275 (www.nitrc.org) (5.9 MB). Figure 2 illustrates axial and coronal views of the T1 (Figure 2 A,C) 276 and T2 (Figure 2 B,D) templates, respectively, at multiple levels throughout the brain, with the 277 labelmap for one hemisphere provided as an overlay. Our labelmap defines 57 ROIs (36 cortical 278 regions and 21 subcortical structures) using the atlas of Saleem & Logothetis (2007) as a guide. 279 All of the labels are bilateral, except for the cerebellum. For reference, the anatomical 280 boundaries are described in Table 2 and volumes of each ROI are reported in Table 3. 281 Structures defined in this labelmap were chosen to facilitate the investigation of cortico-basal 282 ganglia and thalamo-basal ganglia networks (Weiss et al., 2020a), and so less detailed 283 segmentations are provided for regions such as the hindbrain and cerebellum. We also created 284 a condensed version of the labelmap that is designed to be used for analyses where larger ROIs 285 are useful, such as neuroimaging modalities with low spatial resolution like PET. This labelmap 286 contains 17 ROIs (8 cortical regions and 9 subcortical structures), and is also described in Table

287 2. As in the more detailed labelmap, all labels in the condensed labelmap are bilateral except
288 for the cerebellum.

289

### **3.2 Diffusion templates/labelmaps**

291 The diffusion tensor template was constructed independently from 18 individual DW 292 volumes and registered to the shared T1 and T2 reference frame. The tensor template, its derivatives such as FA, MD, AD, and RD, were submitted in NIFTI file format, along with and 293 294 BIDS formatted meta-data, for download on NITRC (www.nitrc.org) (74.7 MB). Figure 3A, C 295 illustrates axial and coronal views of the FA template at multiple levels with the labelmap for 296 one hemisphere provided as an overlay, and Figure 3B, D illustrates the RGB template as an 297 overlay on the T1w template to highlight the spatial co-registration of the DTI and sMRI 298 templates.

299 It is noteworthy that, because the template was built upon individual DW volumes with 300 high resolution and good SNR, our FA template allows delineation of numerous cortical regions 301 such as the dorsolateral prefrontal cortex and subcortical structures including those comprising 302 the basal ganglia, in addition to white matter tracts throughout the brain. Therefore, to further 303 broaden the applicability and take advantage of advancements in scanning technology, we 304 created a labelmap that combines our GM segmentations (Figure 4A) with segmentations of 74 305 WM tracts defined by a previously published macaque DTI atlas (Zakszewski et al., 2014) in 306 Figure 4B. After co-registration of both labelmaps to the template-space, we identified a small 307 number of voxels that were labeled in both the GM and WM labelmaps (Figure 4C, D). These 308 voxels almost entirely fell along the boundaries between tissues (white matter-grey matter-309 CSF), (Figure 4E, F). The resolution of our template, compared to the template by Zakszewski et 310 al. (2014), as well as differences in the age ranges of the animals in each template, required us

311 to refine the boundaries of these ROIs to better match the anatomy. **Table 3** describes all of the

312 ROIs in this labelmap, and reports the volumes of each.

313

### 314 **3.2 Example Applications**

315 We have included several examples of scans collected from individual macagues using a 316 variety of neuroimaging modalities (sMRI, DTI, PET) with co-registered labelmaps (generated by 317 AntsRegistration) to demonstrate potential applications for the ONPRC18 atlas. First, as part of 318 an ongoing longitudinal study of cortico-basal ganglia circuitry in a rhesus macaque model of 319 Huntington's disease, the atlas was applied to a DTI scan acquired from one of the individuals 320 used to build the template after delivery of the mutant HTT gene to the caudate and putamen 321 (Figure 5A). Close manual inspection of the overlays revealed satisfactory results of the 322 registration and accurate anatomical segmentations. To further probe the versatility of this 323 atlas, we also applied it to structural scans (T1w/T2w) that were collected from a juvenile, 3-324 year old Japanese macaque (Macaca fuscata) bearing a CLN7 gene mutation (macaque model of 325 Batten disease) (Figure 5B,C) again with satisfactory registration despite differences in 326 macaque species, age and disease model. Finally, we have applied our consolidated labelmap 327 to 18F-Fallypride PET and 18F-FDG PET images (Figure 5 D,E, respectively) collected from naïve 328 adult rhesus macaques with satisfactory registration, despite the lower spatial resolution of 329 these scans. Both PET scans were collected with co-aligned CT, and the atlas was registered 330 using the CT skull as a reference and then moved into PET space. These examples demonstrate 331 some of the potential applications for this atlas, and suggest that it can be a reliable and 332 versatile tool for different kinds of macaque neuroimaging studies.

333

### 335 **4 Discussion**

336 We created a brain atlas designed to facilitate studies with macaques employing both 337 structural MRI and diffusion weighed imaging (DWI). Template images of the structural contrasts (T2/SPACE, T1/MP-RAGE) and DWI parameter maps (FA, AD, MD, RD, RGB, b0) were 338 339 constructed in the 0.5mm isotropic voxel-spacing reference frame. The labelmap provides 340 segmentations of 57 gray matter ROIs (36 cortical regions and 21 subcortical structures) as well 341 as 74 white matter tracts, and overlays all of the structural and diffusion templates. A 342 condensed version of the labelmap was also created, with 17 larger ROIs, to facilitate imaging 343 modalities with lower spatial resolution, such as fMRI and PET.

344 The templates here were created from in vivo scans, rather than scans of post-mortem 345 fixed-tissue as in Calabrese et al. (2015); Feng et al. (2017); Reveley et al. (2017). The obvious 346 merit to the latter is the ability to employ very lengthy scanning sequences (that would be 347 inappropriate for use with living animals) in order to collect high quality data. Yet, the scanning 348 acquisition parameters employed here resulted in templates with image quality approaching 349 that of many post-mortem datasets. Furthermore, fixation techniques used on post-mortem 350 tissue can alter brain volume and water content, or induce non-rigid distortions, and therefore 351 represent an important limitation in the application of post-mortem atlases to in vivo 352 neuroimaging, and to DWI in particular. In contrast, the templates included here provide references that were acquired from living subjects, a feature that was shown to result in good 353 354 registration accuracy when applying this atlas to other *in vivo* neuroimaging studies with 355 macaques.

The construction of the ONPRC18 templates contrasts from previously available NHP atlases in several additional significant ways. First, rather than mirroring across the midline to create a laterally symmetric template as in Calabrese et al. (2015); Moirano et al. (2019), the

359 ONPRC18 atlas preserved bilateral asymmetry between hemispheres in order to better reflect 360 variability among the macaque population, as suggested by Frey et al. (2011). Second, the 361 demographic distribution of the population ONPRC18 animals is in the middle-age range for 362 macaques (8.1  $\pm$  2.2 years) and includes a higher proportion of females (66%) than many 363 existent population-based templates for adult monkeys: INIA19 template: 8 ± 1.6 years, all 364 males (Rohlfing et al., 2012); NMT template:  $5.5y \pm 1.7$  years, 19% female (Seidlitz et al., 2018); MNI template: 'young adult', 20% female (Frey et al., 2011); 112RM-SL template: 19.9 ± 6.9 365 366 years, 27% females (McLaren et al., 2009); versus UNC-Wisconsin Neurodevelopment template: 367 covers 0-3 years, 50% females (Young et al., 2017); UNC-Emory Infant template: covers 0-368 12months, 50% females (Shi et al., 2016). These differences may be particularly relevant for 369 brain regions and structures with a protracted development that extends beyond puberty or 370 with vulnerability to advancing age, as well as for cross-sectional studies investigating sex 371 differences. Third, new advances in SPACE pulse sequences have made it possible to collect 372 high quality T2w images at identical resolution as T1w MPRAGE images, enabling either 373 contrast to be used as a base anatomical dataset. Given that the T2w contrast provides a better 374 reference for registration of DWI images than T1w (Adluru et al., 2012), the T2w template was 375 selected as the primary reference for the construction of the ONPRC18 DTI- and T1w-templates. 376 Finally, we noted that the contrast of the SPACE images offered some advantages for the 377 anatomical delineation of deep-brain structures surrounded by white matter, such as the basal 378 ganglia and thalamus, as compared to MPRAGE (see Figure 2). Given the relevance of these 379 structures to the circuitry defined in the labelmap, we assigned the T2w template as the 380 primary reference.

381 The ONPRC18 labelmap includes gray matter ROIs that were hand drawn with reference 382 to the cortical and subcortical boundaries described by Saleem and Logothetis (2007). Building

383 on previous work from our group, the INIA19 atlas (Rohlfing et al., 2012), we have made several 384 practical improvements in the labelmap to facilitate in vivo multi-modal neuroimaging studies. 385 First, by manually defining every GM ROI on a template generated from 18 animals, rather than 386 transferring boundaries from a series of 2D histological sections defined on a single animal, we 387 avoided the limitations inherent to generating 3D digital atlases from 2D histological drawings, 388 as described by Reveley et al. (2017); Moirano et al. (2019). This resulted in a labelmap that is 389 well matched to the image resolution of in vivo MRI and guite tolerant of individual variation in 390 neuroanatomy, a feature clearly demonstrated in Figure 5. Similarly, by manually drawing ROIs 391 on both hemispheres of the template rather than mirroring the labelmap across the midline. 392 the ability to describe individual variabilities in hemispheric asymmetry is improved. Lastly, the 393 ONPRC18 labelmap defines many subcortical structures such as the caudate, putamen, internal 394 and external globus pallidus, substantia nigra, as well as lateral and medial subdivisions of the 395 thalamus. This feature contrasts with the widely used D99 labelmap that combines the caudate, 396 putamen, and nucleus accumbens into one striatal ROI, (Reveley et al., 2017; Seidlitz et al., 397 2018). For these reasons, the ONPRC18 atlas will fill an unmet need for NHP imaging resources 398 suitable for studies of cortico-basal ganglia and thalamo-basal ganglia circuitry.

399 To further increase the relevance of this tool for investigations of cortico- and thalamo-400 basal ganglia, we enhanced the ONPRC18 GM labelmap by combining it with segmentations of 401 WM regions defined in a previously published macaque DTI atlas (Zakszewski et al., 2014). The 402 combined GM-WM labelmap eliminates the need for researchers to apply separate GM and 403 WM labelmaps to their datasets, thereby reducing the number of transformations needed since 404 only one registration will be required. Additionally, the increased precision created by the 405 elimination of overlaps in the labels, see Figure 4, enables the same gray and white matter 406 regions to be more consistently identified. This is a unique feature of this atlas, and it will

407 improve the validity of comparisons between scans acquired from the same subject in different408 imaging modalities.

409 We are currently applying the ONPRC18 atlas to a longitudinal study querying cortico-410 and thalamo-basal ganglia circuitry in a newly developed AAV-mediated rhesus macaque model 411 of Huntington's disease (HD) (Weiss et al., 2020a). In this context, we have found preliminary 412 evidence of DTI changes occurring early in disease progression that correlate with cognitive and 413 motor disease phenotypes (Weiss et al., 2020b), progressive reduction in putamen volume 414 (unpublished data), and have begun to quantify changes in regional dopamine receptor binding potentials with F18-Fallypride PET (unpublished data, Figure 5). Additional work is also 415 416 underway using this atlas to assess regional brain atrophy and alterations in white matter 417 microstructure in a Japanese macaque model of Batten's disease (McBride et al., 2018), 418 demonstrating that these templates have wide versatility and can be successfully applied to 419 other species and ages of macaques.

In summary, it is our hope that this new ONPRC18 atlas with corresponding label maps
will serve as an updated resource for NHP researchers to facilitate investigations of macaque
brain circuitry, for developing and characterizing models of neurological disease, assessing the
pre-clinical safety and biodistribution of therapeutics and/or developing imaging signatures of
disease as outcome measures for pre-clinical trials.

Figure 1: Rendering of labelmaps in 3-dimensions. (A) 3D-rendering of GM ROIs created using the 3D segmentation software ITK-SNAP, (Yushkevich et al., 2006). There are 57 cortical and subcortical ROIs defined in this labelmap. (B) Regions from the labelmap were subsequently categorized and combined to create a consolidated labelmap that defines 8 bilateral cortical ROIs and 9 subcortical structures, in order to facilitate neuroimaging modalities with low spatial resolution (i.e. rsfMRI, PET). To ease the visualization of subcortical structures, cortical regions in the right hemisphere were made transparent in this figure.

433

434 **Figure 2: sMRI templates.** A series of five axial and coronal sections displayed in neurological

435 orientation through the T1 templates (A, C) and the T2 templates (B, D). For ease of viewing,

436 the labelmap overlays are drawn only on the right hemisphere. Abbreviations: A, anterior; I,

437 inferior; L, left; P, posterior; R, right; S, superior.

438

Figure 3: DTI Templates. A series of five axial and coronal sections displayed in neurological
orientation through the FA template (A, C). For ease of viewing, the labelmap overlays are
drawn only on the right hemisphere of the FA templates. To highlight the spatial co-registration
of the DTI template with the sMRI templates (B, D) show visualization of RGB template as an
overlay on the T1w template. *Abbreviations: A, anterior; I, inferior; L, left; P, posterior; R, right; S, superior.*

445

Figure 4: Combing gray and white matter labelmaps. (A) illustrates our gray matter (GM) labelmap
overlaying the T2 template. We used a published diffusion tensor-based rhesus macaque atlas
(Zakszewski et al., 2014) to identify and segment white matter tracts on our FA template, illustrated in
(B). In order to combine these two labelmaps, using FSL tools, we first identified overlaps (i.e. doublelabeled voxels) between the WM labelmap and our GM labelmap, these voxels are illustrated in blue in

451 (C) and (D). ITK-SNAP was used to manually categorize these voxels as belonging to WM or GM, and the
452 results of this classification is illustrated in (E) and (F), with blue voxels categorized as GM and magenta
453 voxels categorized as WM. Finally, the categorized voxels were re-assigned to the appropriate GM/WM
454 labelmap and ROI, and the two labelmaps were then consolidated into one. The results of this
455 combination are illustrated in (G) and (H), overlaying the T2 and FA templates. *Abbreviations: I, inferior;*456 *L, left; P, posterior; R, right.*

458 Figure 5: Example application of multimodal templates. A series of axial sections with co-registered 459 labelmaps that illustrate applications of the ONPRC18 atlas to scans collected from individual macagues 460 using a variety of neuroimaging contrasts and modalities (DTI, sMRI, PET). Label maps were generated 461 by AntsRegistration software version 2.1; (http://stnava.github.io/ANTs/). (A) DTI scan acquired from 462 one of the individuals in the template at a later timepoint. (B, C) sMRI scans (T1w/T2w) that were 463 collected from a juvenile (3yo) Japanese macaque (Macaca fuscata). (D, E) 18F-Fallypride PET and 18F-464 FDG PET in a naïve female rhesus macaque. These examples demonstrate some of the potential 465 applications for this atlas, and suggest that it can be a reliable and versatile tool for a wide variety of 466 different kinds of macaque neuroimaging studies.

467 <b>Table 1</b> .	57	Table 1.
----------------------	----	----------

468

Monkey	Sex	Age (years)	Weight (kg)
RH-1	F	13.47	9.9
RH-2	F	12.92	7.2
RH-3	F	12.21	7.4
RH-4	F	11.91	8.9
RH-5	F	11.76	6
RH-6	F	11.75	5.1
RH-7	F	10.03	5.8
RH-8	F	9.86	7.4
RH-9	F	8.92	8.3
RH-10	F	8.73	5.9
RH-11	F	8.69	6.5
RH-12	F	7.87	6.1
RH-13	М	9.97	9.6
RH-14	М	7.75	10
RH-15	М	7.62	11.8
RH-16	М	7.52	8.8
RH-17	М	7.01	10.9
RH-18	М	5.89	10.7

469

Table 1: Demographic information for study animals. Scans from 18 individual rhesus macaques contributed to these templates. At the time of the scans, the animals were 6-13 years old, and consisted of both males (n=6) and females (n=12). There were slight age differences between the sexes, with females a bit older than males.

475 **Table 2.** 

Atlas Region	Abbreviation	Label Number	Anatomical boundaries (as defined by Salem & Logothetis)	Consolidated Atlas Regions	Label Numbei
Dorsolateral	DLPFC-L	1			
Prefrontal Cortex	DLPFC-R	2	8A, 8Bd, 8Bs, 9d, 10mrD, 46		
Ventrolateral	VLPFC-L	3			
Prefrontal Cortex	VLPFC-R	4	12, 44, 45		
Orbital Prefrontal	OPFC-L	5	11 10		
Cortex	OPFC-R	6	11, 13	Fuenchal	1.2
Ventral Medial	VMPFC-L	7	10	Frontal	1,2
Prefrontal Cortex	VMPFC-R	8	10mrV, 14, 25, 32		
Dorsal Medial	DMPFC-L	9			
Prefrontal Cortex	DMPFC-R	10	8Bm, 9m, 10mrM,		
Anterior Cingulate	ACC-L	11	24		
Cortex	ACC-R	12	24		
Dorsal Premotor	DPMC-L	13	F2, F7		
Cortex	DPMC-R	14	F2, F7		
Ventral Premotor	VPMC-L	15			
Cortex	VPMC-R	16	F4, F5	N 4 st su	3,4
Supplemental Motor	SMC-L	17		Motor	
Cortex	SMC-R	18	F3, F6		
Mater Cartov	MC-L	19	F1		
Motor Cortex	MC-R	20	- F1		
Superior Temporal	STC-L	21	AL, CL, CM, ML, MST, PGa, R,		
Cortex	STC-R	22	RM, RT, RTL, RTM, RTp, STG, TAa, TEO, TG, TPO, Tpt		
Inferior Temporal	ITC-L	23			
Cortex	ITC-R	24	FST, IPa, TE, TF, TFO, TH,	Tenerser	
<b></b>	RC-L	25		Temporal	5,6
Rhinal Cortex	RC-R	26	35, 36, EC		
	IC-L	27	la, lai, lal, lam, lapl, lapm, ld,		
Insular Cortex	IC-R	28	lg, Pi, Ri,		
Somatosensory	SSC-L	29			
Cortex	SSC-R	30	1-2, 3a/b, G, PrCO, SII,		
<b>-</b>	PC-L	31	7, AIP, LIP, LOP, MIP, PIP, PO,		
Parietal Cortex	PC-R	32	VIP,	Parieto-	
Posterior Cingulate	PCC-L	33	occipit		7,8
Cortex	PCC-R	34	23, 29, 30, 31,		
<b>.</b>	OCC-L	35			1
Occipital Cortex	OCC-R	36	DP, MT, V1, V2, V3, V4,		

Atlas Region	Abbreviation	Label Number	Anatomical boundaries (as defined by Salem & Logothetis)	Consolidated Atlas Regions	Label Number
Caudate	CD-L	37		Caudate	9,10
Caudate	CD-R	38		Caudate	9,10
Putamen	PUT-L	39		Putamen	11 12
Pulamen	PUT-R	40		Putamen	11,12
Lateral Thalamus	Lat Th-L	41	cl, cnMD, LD, LP, Pf, Pl, PL, PM, pulo, VA, VAmc, VL, VPI,		
	LatTh-R	42	VPlc, VPM, VPMpc	Thalamus	13, 14
Madial Thalamus	MdTh-L	43	MD Dep	malamus	13, 14
Medial Thalamus	MdTh-R	44	MD, Pcn		
	HIPP-L	45	a ll av bői a lala		15 16
Hippocampus	HIPP-R	46	all subfields	Hippocampus	15, 16
Amurada la	AMY-L	47	all nuclei		
Amygdala	AMY-R	48	an nuclei		
Substantia nigra	SN-L	49	pars compacta, pars		
Substantia nigra	SN-R	50	reticulata		
Globus Pallidus	GPI-L	51			
Internal	GPI-R	52			
Globus Pallidus	GPE-L	53			
External	GPE-R	54			
l et ventuieles	LatV-L	55			
Lat ventricles	LatV-R	56			
Cerebellum	Cbm	57		Cerebellum	17

476

477 Table 2: Description of ROI anatomical boundaries in labelmaps. All regions were drawn by hand on the 478 T2 template using the 3D segmentation software ITK-SNAP (Yushkevich et al., 2006). Cortical and 479 subcortical ROIs were defined on coronal sections according to the atlas by Saleem & Logothetis (2007), 480 and verified in the axial and sagittal planes. Regions from the labelmap were subsequently categorized 481 and combined to create a consolidated labelmap that defines 8 bilateral cortical ROIs and 9 subcortical 482 structures. Abbreviations: 1-2, somatosensory areas 1 and 2; 3a/b, somatosensory areas 3a and 3b; 7, 483 area 7 (all subdivisions); 8A, area 8A; 8Bd, area 8B, dorsal subdivision; 8Bm, area 8B, medial subdivision; 484 8Bs, area 8B in the arcuate sulcus; 9d, area 9, dorsal subdivision; 9m, area 9, medial subdivision; 10mrD, 485 area 10mr dorsal subdivision; 10mrM, area 10mr medial subdivision; 10mrV, area 10mr ventral 486 subdivision; 111, area 111; 11m, area 11m; 121, area 121; 12m, area 12m; 12, area 12 (all subdivisions); 13, 487 area 13 (all subdivisions); 14, area 14 (all subdivisions); 23, area 23 (all subdivisions); 24, area 24 (all 488 subdivisions); 25, area 25; 29, area 29 (retrosplenial cortex); 30, area 30 (retrosplenial cortex); 31, area 489 31; 32, area 32 ; 35, area 35; 36, area 36 (all subdivisions); 44, area 44; 45, area 45; 46, area 46 (all 490 subdivisions); AIP, anterior intraparietal area; AL, anterior lateral, belt region of the auditory cortex; CL, 491 caudal lateral, belt region of the auditory cortex; cl, central lateral nucleus; CM, caudomedial, belt 492 region of the auditory cortex; cnMD, centromedian nucleus; DP, dorsal prelunate area; EC, entorhinal 493 cortex (all subdivisions); F1, agranular frontal area F1; F2, agranular frontal area F2; F3, agranular frontal 494 area F3; F4, agranular frontal area F4; F5, agranular frontal area F5; F6, agranular frontal area F6; F7, 495 agranular frontal area F7; FST, floor of superior temporal area; G, gustatory cortex; la, agranular insula;

496 lai, intermediate agranular insula area; lal, lateral agranular insula area; lam, medial agranular insula 497 area: *lapl.* posterolateral agranular insula area: *lapm.* posteromedial agranular insula area: *ld.* 498 dysgranular insula; Iq, granular insula; IPa, area IPa (sts fundus); LD, lateral dorsal nucleus; LIP, lateral 499 intraparietal area (all subdivisions); LOP, lateral occipital parietal area; LP, lateral posterior nucleus; MD, 500 medial dorsal nucleus (all subdivisions); MIP, medial intraparietal area; ML, middle lateral, belt region of 501 the auditory cortex; MST, medial superior temporal area; MT, middle temporal area; Pcn, paracentral 502 nucleus; Pf, parafascicular nucleus; PGa, area PGa; PI, inferior pulvinar; Pi, parainsular area; PIP, 503 posterior intraparietal area; PL, lateral pulvinar; PM, medial pulvinar; PO, parieto-occipital area; PrCO, 504 precentral opercular area; pulo, pulyinar oralis nucleus; R, rostral, core region of the auditory cortex; Ri. 505 retroinsula; RM, rostromedial, belt region of the auditory cortex; RT, rostrotemporal, core region of the 506 auditory cortex; RTL, lateral rostrotemporal, belt region of the auditory cortex; RTM, medial 507 rostrotemporal, belt region of the auditory cortex; RTp, rostrotemporal (polar); SII, secondary 508 somatosensory area (S2); STG, superior temporal gyrus; TAa, area TAa (sts dorsal bank); TE, area TE (all 509 subdivisions); TEO, area TEO; TF, area TF of the parahippocampal cortex; TFO, area TFO of the 510 parahippocampal cortex, TG, area TG, temporal pole (all subdivisions); TH, area TH of the 511 parahippocampal cortex; TPO, area TPO (sts dorsal bank); Tpt, temporo-parietal area; V1, visual area 1 512 (primary visual cortex); V2, visual area 2; V3, visual area 3 (all subdivisions); V4, visual area 4 (all 513 subdivisions); VA, ventral anterior nucleus; VAmc, ventral anterior nucleus, magnocellular division; VIP, 514 ventral intraparietal area; VL, ventral lateral nucleus (all subdivisions); VPI, ventral posterior inferior 515 nucleus; VPLc, ventral posterior lateral caudal nucleus; VPM, ventral posterior medial nucleus; VPMpc, 516 ventral posterior medial nucleus, parvicellular division. Abbreviations from the atlas of Saleem and 517 Logothetis (2007).

### 520 **Table 3.**

521

Label Id	Structure	Abbreviation	Volume (mm <sup>3</sup> )
1	Dorsolateral Prefrontal Cortex - Left	DLPFC_Left	986.625
2	Dorsolateral Prefrontal Cortex - Right	DLPFC_Right	985
3	Ventrolateral Prefrontal Cortex - Left	VLPFC_Left	377.75
4	Ventrolateral Prefrontal Cortex - Right	VLPFC_Right	371.75
5	Orbital Prefrontal Cortex - Left	OPFC_Left	370.5
6	Orbital Prefrontal Cortex - Right	OPFC_Right	376.125
7	Ventral Medial Prefrontal Cortex - Left	VMPFC_Left	335.125
8	Ventral Medial Prefrontal Cortex - Right	VMPFC_Right	326.125
9	Dorsal Medial Prefrontal Cortex - Left	DMPFC_Left	199.125
10	Dorsal Medial Prefrontal Cortex - Right	DMPFC_Right	197
11	Anterior Cingulate Cortex - Left	ACC_Left	341.75
12	Anterior Cingulate Cortex - Right	ACC_Right	337.75
13	Dorsal Premotor Cortex - Left	DPMC_Left	394.875
14	Dorsal Premotor Cortex - Right	DPMC_Right	394.875
15	Ventral Premotor Cortex - Left	VPMC_Left	444.375
16	Ventral Premotor Cortex - Right	VPMC_Right	437.75
17	Supplemental Motor Cortex - Left	SMC_Left	394.875
18	Supplemental Motor Cortex - Right	SMC_Right	389.75
19	Motor Cortex - Left	MC_Left	538.25
20	Motor Cortex - Right	MC_Right	557
21	Superior Temporal Cortex - Left	STC_Left	1632.12
22	Superior Temporal Cortex - Right	STC_Right	1643.38
23	Inferior Temporal Cortex - Left	ITC_Left	1391
24	Inferior Temporal Cortex - Right	ITC_Right	1373.88
25	Rhinal Cortex - Left	RC_Left	226.25
26	Rhinal Cortex - Right	RC_Right	225.5
27	Insular Cortex - Left	IC_Left	290.625
28	Insular Cortex - Right	IC_Right	288.5
29	Somatosensory Cortex - Left	SSC_Left	980.875
30	Somatosensory Cortex - Right	SSC_Right	971.75
31	Parietal Cortex - Left	PC_Left	1878.12
32	Parietal Cortex - Right	PC_Right	1857
33	Posterior Cingulate Cortex - Left	PCC_Left	381.75
34	Posterior Cingulate Cortex - Right	PCC_Right	376.75
35	Occipital Cortex - Left	OCC_Left	4205.62
36	Occipital Cortex - Right	OCC_Right	4216.88
37	Caudate - Left	CD_Left	511.625
38	Caudate - Right	CD_Right	511.875
39	Putamen - Left	PUT_Left	764.25
40	Putamen - Right	PUT_Right	754.625

Label Id	Structure	Abbreviation	Volume (mm <sup>3</sup>
41	Lateral Thalamus - Left	LatTH_Left	476.875
42	Lateral Thalamus - Right	LatTh_Right	476.125
43	Medial Thalamus - Left	MdTh_Left	132.75
44	Medial Thalamus - Right	MdTh_Right	134
45	Hippocampus - Left	HIPP_Left	400
46	Hippocampus - Right	HIPP_Right	400.375
47	Amygdala - Left	AMY_Left	198.125
48	Amygdala - Right	AMY_Right	198.875
49	Substantia nigra - Left	SN_Left	26.625
50	Substantia nigra - Right	SN_Right	26.5
51	Globus Pallidus Internal - Left	GPI_Left	70.125
52	Globus Pallidus Internal - Right	GPI_Right	71.25
53	Globus Pallidus External - Left	GPE_Left	153.625
54	Globus Pallidus External - Left	GPE_Right	154.625
55	Lateral ventricle - Left	LatVentricle_Left	314
56	Lateral ventricle - Right	LatVentricle_Right	328.625
57	Cerebellum	Cerebellum	6992.75
58	Middle Cerebellar Peduncle	МСР	564.75
59	Pontine Crossing Tract	РСТ	80.375
60	Genu of Corpus Callosum	GCC	430.25
61	Body of Corpus Callosum	BCC	879.875
62	Splenium of Corpus Callosum	SCC	649
63	Fornix	FX	105.75
64	Anterior Commissure	AC	183
65	Pyramidal Tracts	РТ	48.375
66	Corticospinal Tract - Right	CST-R	221
67	Corticospinal Tract - Left	CST-L	182.125
68	Medial Lemniscus - Right	ML-R	95.125
69	Medial Lemniscus - Left	ML-L	75.875
70	Inferior Cerebellar Peduncle - Right	ICP-R	40.875
71	Inferior Cerebellar Peduncle - Left	ICP-L	35.125
72	Superior Cerebellar Peduncle - Right	SCP-R	123.5
73	Superior Cerebellar Peduncle - Left	SCP-L	120
74	Cerebral Peduncle - Right	CP-R	164.75
75	Cerebral Peduncle - Left	CP-L	144.5
76	Anterior Limb of the Internal Capsule - Right	ALIC-R	269.375
77	Anterior Limb of the Internal Capsule - Left	ALIC-L	244.75
78	Posterior Limb of the Internal Capsule - Right	PLIC-R	351.5
79	Posterior Limb of the Internal Capsule - Left	PLIC-L	369.375
80	Retrolenticular Limb of the Internal Capsule - Right	RLIC-R	201.125
81	Retrolenticular Limb of the Internal Capsule - Left	RLIC-L	223.75

Label Id	Structure	Abbreviation	Volume (mm <sup>³</sup>
82	Anterior Corona Radiata - Right	ACR-R	372.125
83	Anterior Corona Radiata - Left	ACR-L	391.875
84	Superior Corona Radiata - Right	SCR-R	528.5
85	Superior Corona Radiata - Left	SCR-L	508.5
86	Posterior Corona Radiata - Right	PCR-R	441.25
87	Posterior Corona Radiata - Left	PCR-L	460.625
88	Posterior Thalamic Radiation - Right	PTR-R	484.125
89	Posterior Thalamic Radiation - Left	PTR-L	481.875
90	Sagittal Striatum - Right	SS-R	252.875
91	Sagittal Striatum - Left	SS-L	277
92	External Capsule - Right	EC-R	506.5
93	External Capsule - Left	EC-L	530.25
94	Superior Cingulum - Right	CgC-R	142.75
95	Superior Cingulum - Left	CgC-L	132.75
96	Perihippocampal Cingulum - Right	CgH-R	108.125
97	Perihippocampal Cingulum - Left	CgH-L	119.125
98	Stria Terminalus - Right	ST-R	219.75
99	Stria Terminalus - Left	ST-L	237.5
100	Superior Longitudinal Fasciculus - Right	SLF-R	487.25
101	Superior Longitudinal Fasciculus - Left	SLF-L	529
102	Superior Fronto-Occipital Fasciculus - Right	SFO-R	41.625
103	Superior Fronto-Occipital Fasciculus - Left	SFO-L	33.875
104	Uncinate Fasciculus - Right	UNC-R	125.5
105	Uncinate Fasciculus - Left	UNC-L	127.875
106	Tapetum - Right	TAP-R	43
107	Tapetum - Left	TAP-L	34
108	Dorsal Prefrontal WM - Right	DPF-R	231.625
109	Dorsal Prefrontal WM - Left	DPF-L	241
110	Ventral Prefrontal WM - Right	VPF-R	56.75
111	Ventral Prefrontal WM - Left	VPF-L	65.25
112	Dorsal Posterior Corona Radiata - Right	DPCR-R	483.125
113	Dorsal Posterior Corona Radiata - Left	DPCR-L	486
114	Medial Longitudinal Fasciculus - Right	MLF-R	38.375
115	Medial Longitudinal Fasciculus - Left	MLF-L	36.625
116	Central Tegmental - Right	CTG-R	70.625
117	Central Tegmental - Left	CTG-L	73.875
118	Inferior Frontal Gyrus WM - Right	IFG-WM-R	204.25
119	Inferior Frontal Gyrus WM - Left	IFG-WM-L	236.125
120	Superior Temporal Gyrus WM - Right	STG-WM-R	42.375
121	Superior Temporal Gyrus WM - Left	STG-WM-L	49.875
122	Middle Temporal Gyrus WM - Right	MTG-WM-R	174.375

Label Id	Structure	Abbreviation	Volume (mm³)
123	Middle Temporal Gyrus WM - Left	MTG-WM-L	184.625
124	Adjacent Thalamus WM - Right	AT-WM-R	54.5
125	Adjacent Thalamus WM - Left	AT-WM-L	56.625
126	Adjacent Amygdala White Matter - Right	AA-WM-R	198.375
127	Adjacent Amygdala White Matter - Left	AA-WM-L	177.5
128	Midbrain White Matter WM - Right	MB-WM-R	102.375
129	Midbrain White Matter WM - Left	MB-WM-L	85.75

522

523

**Table 3: Description of ROIs in Combined GM/WM labelmap**. We used ROIs defined by a published diffusion tensor-based rhesus macaque atlas to identify and segment WM tracts on our FA template (Zakszewski et al., 2014). These WM ROIs were combined with our GM ROIs (described in Table 2) into one consolidated labelmap that is described by this table, as well as the volume (in mm<sup>3</sup>) of each ROI in the labelmap.

529	ACKNOWLEDGEMENTS
530	We sincerely thank the entire ONPRC Division of Comparative Medicine for the outstanding
531	care of our rhesus macaques, with special acknowledgement of the efforts that Lauren Drew
532	Martin, Theodore Hobbs, Michael Reusz, Brandy Dozier, Alona Kvitky, and Isabel Bernstein
533	contributed to this work. This research was supported by NIH/NINDS R01NS099136, NIH/NINDS
534	R24 NS104161 (NHP Resource for Preclinical Studies of Neurodegenerative Disease), NIH/NINDS
535	F32NS110149-01, NIH/NIAAA U24AA025473, the Bev Hartig Huntington's Disease Foundation
536	and a grant from the M.J. Murdock Charitable Trust.
537 538	Conflicts of Interest: none
539	
540	Funding Sources: NIH/NINDS R01NS099136, NIH/NINDS R24 NS104161 (NHP Resource for
541	Preclinical Studies of Neurodegenerative Disease), NIH/NINDS F32NS110149-01, NIH/NIAAA
542	U24AA025473, the Bev Hartig Huntington's Disease Foundation and a grant from the M.J.
543	Murdock Charitable Trust.
544 545 546	

	available under aCC-BY-NC-ND 4.0 International license.
548	REFERENCES
549	
550	Adluru N, Zhang H, Fox AS, Shelton SE, Ennis CM, Bartosic AM, Oler JA, Tromp do PM,
551	Zakszewski E, Gee JC, Kalin NH, Alexander AL (2012) A diffusion tensor brain template
552	for rhesus macaques. Neuroimage 59:306-318.
553	Andersson JL, Sotiropoulos SN (2016) An integrated approach to correction for off-resonance
554	effects and subject movement in diffusion MR imaging. Neuroimage 125:1063-1078.
555	Andersson JL, Skare S, Ashburner J (2003) How to correct susceptibility distortions in spin-echo
556	echo-planar images: application to diffusion tensor imaging. Neuroimage 20:870-888.
557	Avants BB, Epstein CL, Grossman M, Gee JC (2008) Symmetric diffeomorphic image registration
558	with cross-correlation: evaluating automated labeling of elderly and neurodegenerative
559	brain. Med Image Anal 12:26-41.
560	Avants BB, Yushkevich P, Pluta J, Minkoff D, Korczykowski M, Detre J, Gee JC (2010) The optimal
561	template effect in hippocampus studies of diseased populations. Neuroimage 49:2457-
562	2466.
563	BrainInfo (1991-present) In: National Primate Research Center, University of Washington.
564	Calabrese E, Badea A, Coe CL, Lubach GR, Shi Y, Styner MA, Johnson GA (2015) A diffusion
565	tensor MRI atlas of the postmortem rhesus macaque brain. Neuroimage 117:408-416.
566	Feng L, Jeon T, Yu Q, Ouyang M, Peng Q, Mishra V, Pletikos M, Sestan N, Miller MI, Mori S,
567	Hsiao S, Liu S, Huang H (2017) Population-averaged macaque brain atlas with high-
568	resolution ex vivo DTI integrated into in vivo space. Brain Struct Funct 222:4131-4147.
569	Frey S, Pandya DN, Chakravarty MM, Bailey L, Petrides M, Collins DL (2011) An MRI based
570	average macaque monkey stereotaxic atlas and space (MNI monkey space). Neuroimage
571	55:1435-1442.
572	McBride JL, Neuringer M, Ferguson B, Kohama SG, Tagge IJ, Zweig RC, Renner LM, McGill TJ,
573	Stoddard J, Peterson S, Su W, Sherman LS, Domire JS, Ducore RM, Colgin LM, Lewis AD
574	(2018) Discovery of a CLN7 model of Batten disease in non-human primates. Neurobiol
575	Dis 119:65-78.
576	McLaren DG, Kosmatka KJ, Oakes TR, Kroenke CD, Kohama SG, Matochik JA, Ingram DK,
577	Johnson SC (2009) A population-average MRI-based atlas collection of the rhesus
578	macaque. Neuroimage 45:52-59.
579	Moirano JM, Bezgin GY, Ahlers EO, Kotter R, Converse AK (2019) Rhesus Macaque Brain Atlas
580	Regions Aligned to an MRI Template. Neuroinformatics 17:295-306.
581	Mugler JP, 3rd, Brookeman JR (1990) Three-dimensional magnetization-prepared rapid
582	gradient-echo imaging (3D MP RAGE). Magn Reson Med 15:152-157.
583	Mugler JP, 3rd, Bao S, Mulkern RV, Guttmann CR, Robertson RL, Jolesz FA, Brookeman JR (2000)
584	Optimized single-slab three-dimensional spin-echo MR imaging of the brain. Radiology
585	216:891-899.
586	Reveley C, Gruslys A, Ye FQ, Glen D, Samaha J, B ER, Saad Z, A KS, Leopold DA, Saleem KS (2017)
587	Three-Dimensional Digital Template Atlas of the Macaque Brain. Cereb Cortex 27:4463-
588	
589	Rohlfing T, Kroenke CD, Sullivan EV, Dubach MF, Bowden DM, Grant KA, Pfefferbaum A (2012)
590	The INIA19 Template and NeuroMaps Atlas for Primate Brain Image Parcellation and
591	Spatial Normalization. Front Neuroinform 6:27.
592	Saleem KS, Logothetis N (2007) A combined MRI and histology atlas of the rhesus monkey brain
593	in stereotaxic coordinates. London ; Burlington, MA: Academic.

594	Seidlitz J, Sponheim C, Glen D, Ye FQ, Saleem KS, Leopold DA, Ungerleider L, Messinger A (2018)
595	A population MRI brain template and analysis tools for the macaque. Neuroimage
596	170:121-131.
597	Shi Y, Budin F, Yapuncich E, Rumple A, Young JT, Payne C, Zhang X, Hu X, Godfrey J, Howell B,
598	Sanchez MM, Styner MA (2016) UNC-Emory Infant Atlases for Macaque Brain Image
599	Analysis: Postnatal Brain Development through 12 Months. Front Neurosci 10:617.
600	Tustison NJ, Avants BB, Cook PA, Zheng Y, Egan A, Yushkevich PA, Gee JC (2010) N4ITK:
601	improved N3 bias correction. IEEE Trans Med Imaging 29:1310-1320.
602	Veraart J, Novikov DS, Christiaens D, Ades-Aron B, Sijbers J, Fieremans E (2016) Denoising of
603	diffusion MRI using random matrix theory. Neuroimage 142:394-406.
604	Weiss AR, Liguore WA, Domire JS, Button D, McBride JL (2020a) Intra-striatal AAV2.retro
605	administration leads to extensive retrograde transport in the rhesus macaque brain:
606	implications for disease modeling and therapeutic development. Sci Rep 10:6970.
607	Weiss AR, Brandon KR, Liguore WA, Liu Z, Wang X, Kroenke CD, McBride JL (2020b) AAV2.retro-
608	mediated delivery of mHTT in the rhesus macaque caudate and putamen leads to the
609	progressive development of dyskinesias, fine motor skill decline, and impairments in
610	working memory. In: Annual CHDI Foundation Meeting. Palm Springs, CA.
611	Yeo BT, Sabuncu MR, Desikan R, Fischl B, Golland P (2008) Effects of registration regularization
612	and atlas sharpness on segmentation accuracy. Med Image Anal 12:603-615.
613	Young JT, Shi Y, Niethammer M, Grauer M, Coe CL, Lubach GR, Davis B, Budin F, Knickmeyer RC,
614	Alexander AL, Styner MA (2017) The UNC-Wisconsin Rhesus Macaque
615	Neurodevelopment Database: A Structural MRI and DTI Database of Early Postnatal
616	Development. Front Neurosci 11:29.
617	Yushkevich PA, Piven J, Hazlett HC, Smith RG, Ho S, Gee JC, Gerig G (2006) User-guided 3D
618	active contour segmentation of anatomical structures: significantly improved efficiency
619	and reliability. Neuroimage 31:1116-1128.
620	Zakszewski E, Adluru N, Tromp do PM, Kalin N, Alexander AL (2014) A diffusion-tensor-based
621	white matter atlas for rhesus macaques. PLoS One 9:e107398.
622	Zhang H, Avants BB, Yushkevich PA, Woo JH, Wang S, McCluskey LF, Elman LB, Melhem ER, Gee
623	JC (2007) High-dimensional spatial normalization of diffusion tensor images improves
624	the detection of white matter differences: an example study using amyotrophic lateral
625	sclerosis. IEEE Trans Med Imaging 26:1585-1597.
626	
627	
628	
629	
630	

### Graphical Abstract

# **ONPRC18 Multimodal Neuroimaging Atlas for macaques**

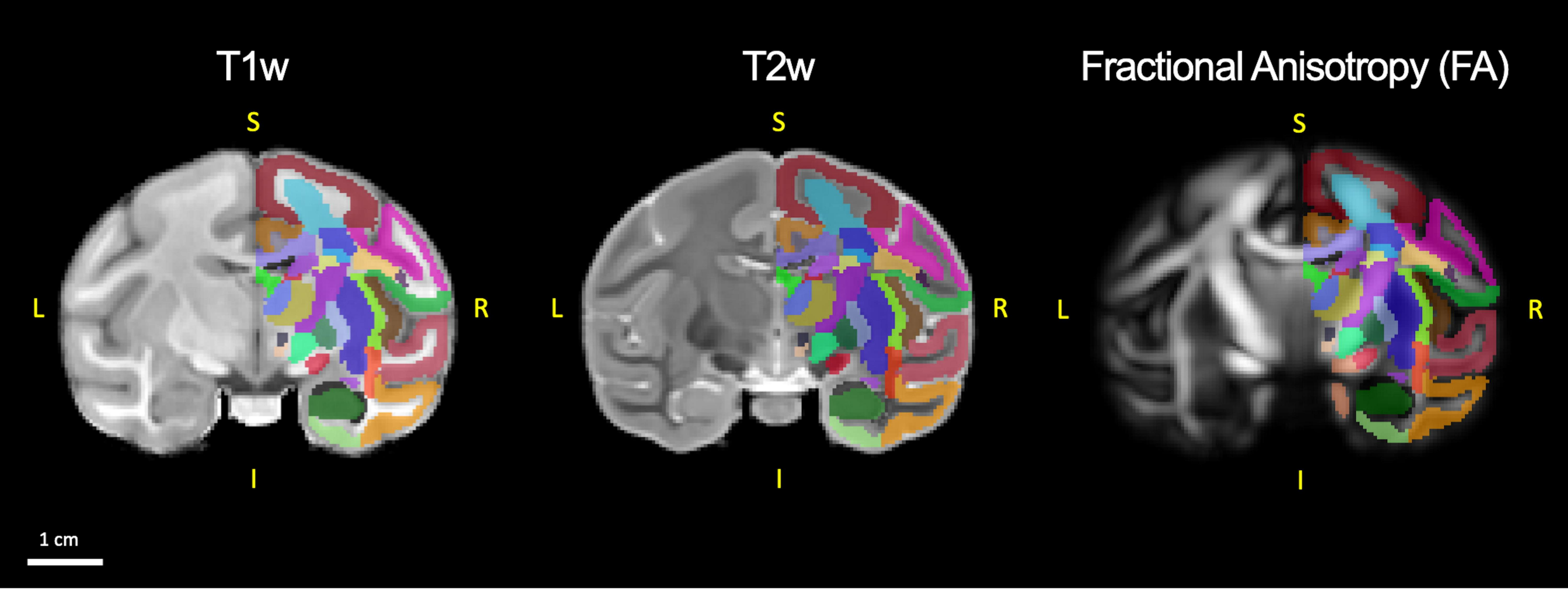


## Figure 1.

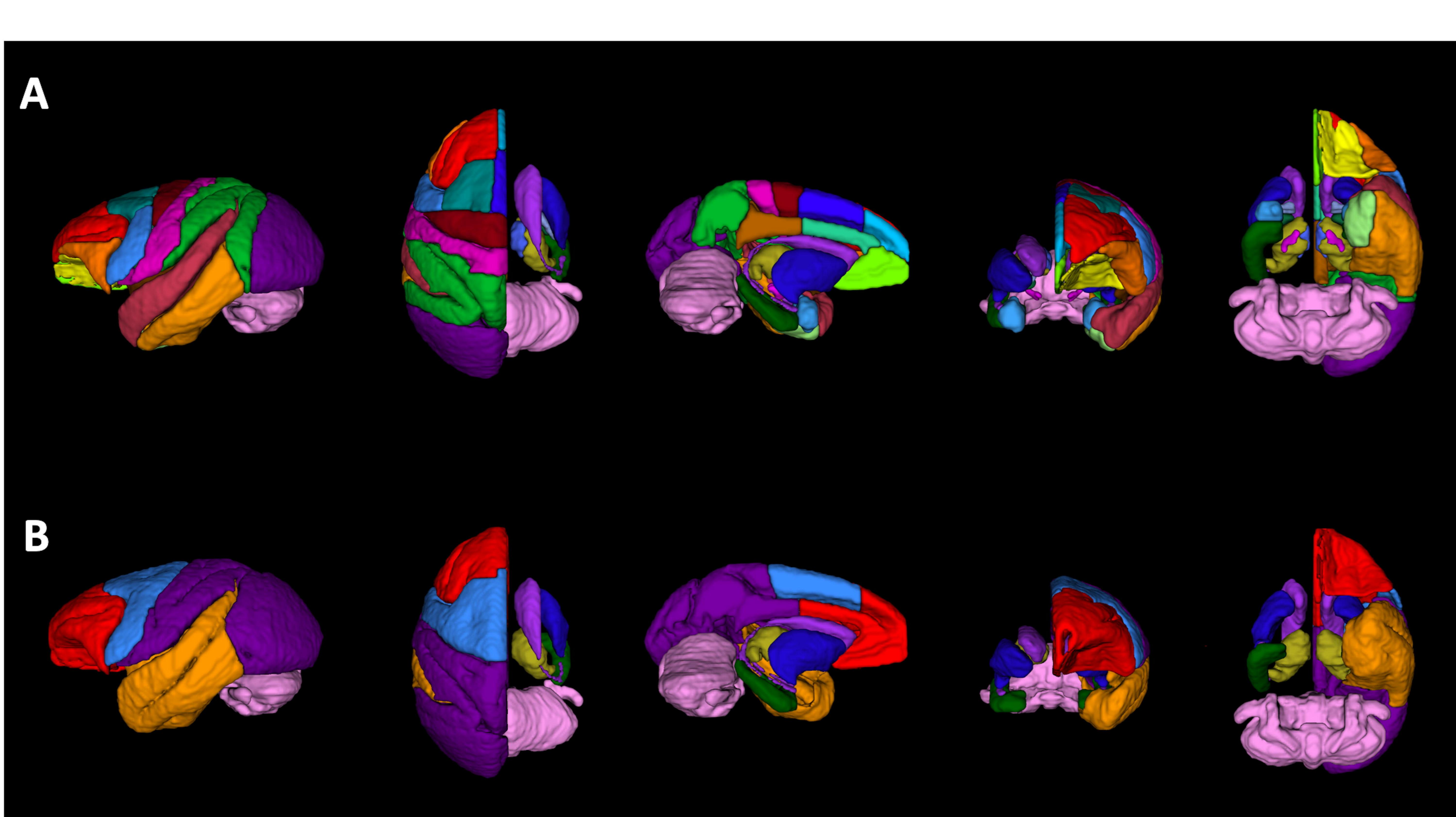
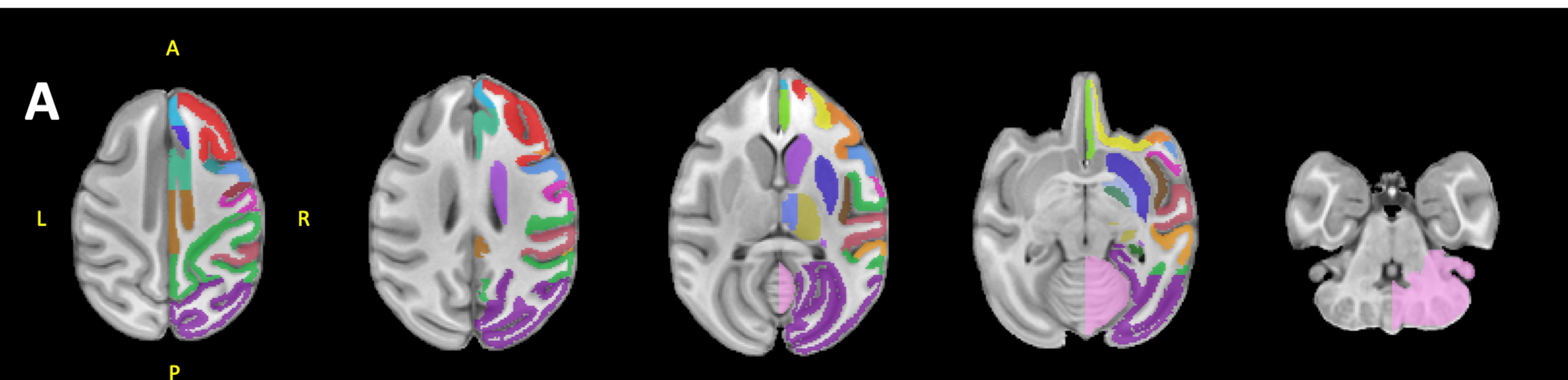


**Figure 1: Rendering of labelmaps in 3-dimensions**. (A) 3D-rendering of GM ROIs created using the 3D segmentation software ITK-SNAP, (Yushkevich et al., 2006). There are 57 cortical and subcortical ROIs defined in this labelmap. (B) Regions from the labelmap were subsequently categorized and combined to create a consolidated labelmap that defines 8 bilateral cortical ROIs and 9 subcortical structures, in order to facilitate neuroimaging modalities with low spatial resolution (i.e. rsfMRI, PET). To ease the visualization of subcortical structures, cortical regions in the right hemisphere were made transparent in this figure.

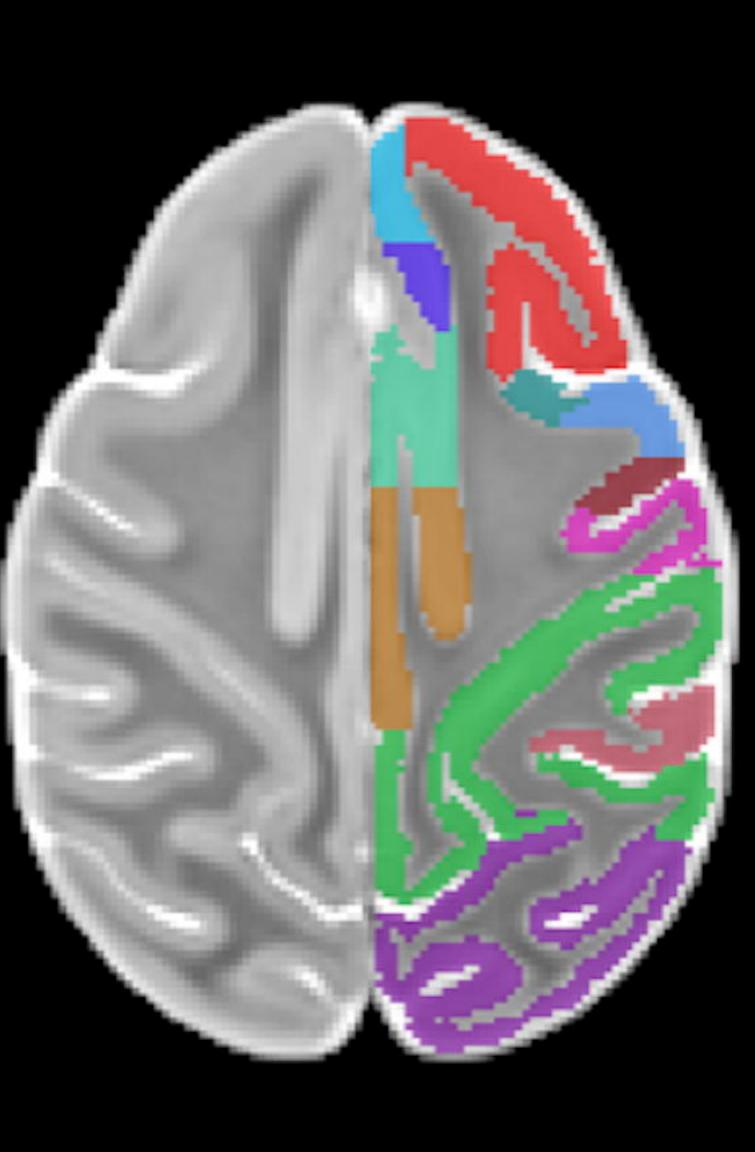
bioRxiv preprint doi: https://doi.org/10.1101/2020.10.06.323063; this version posted October 8, 2020. The copyright holder for this preprint (which was not certified by peer review) is the author/funder, who has granted bioRxiv a license to display the preprint in perpetuity. It is made

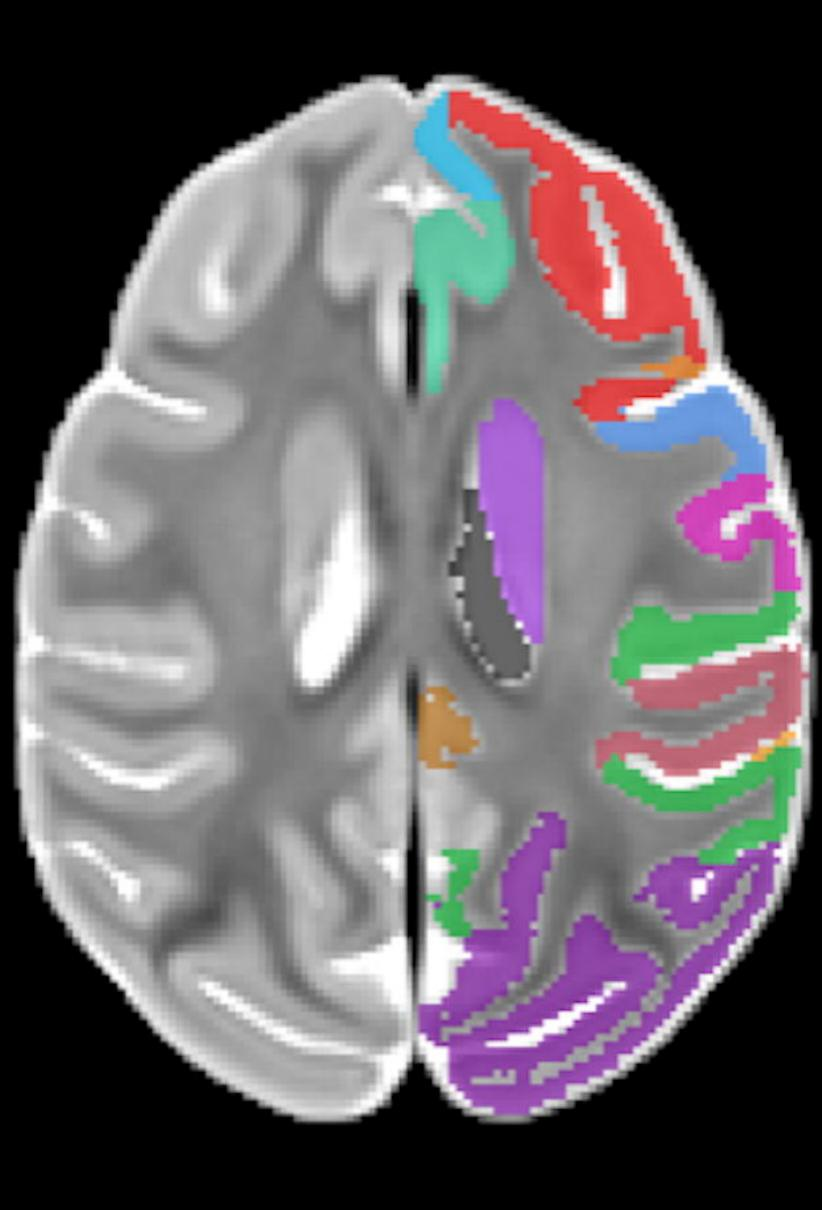
available under aCC-BY-NC-ND 4.0 International license.

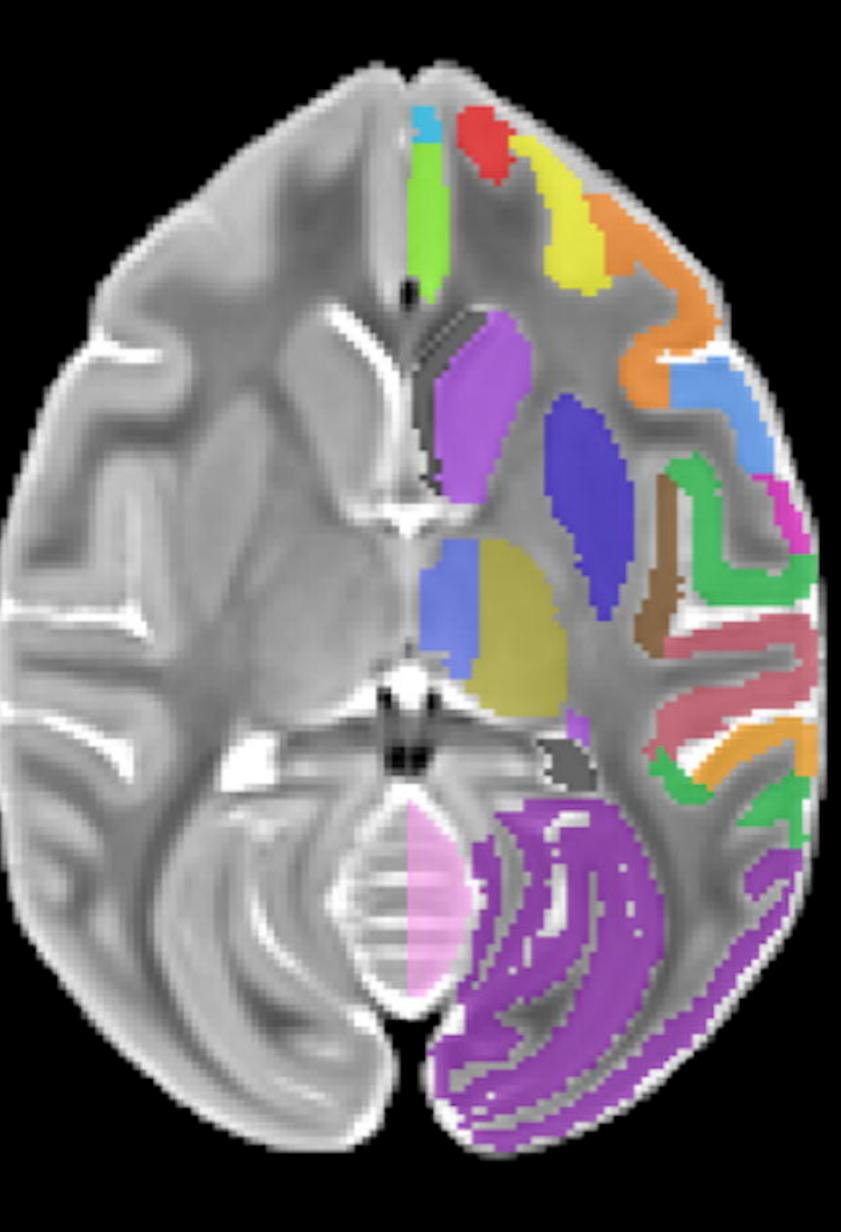
Figure 2.

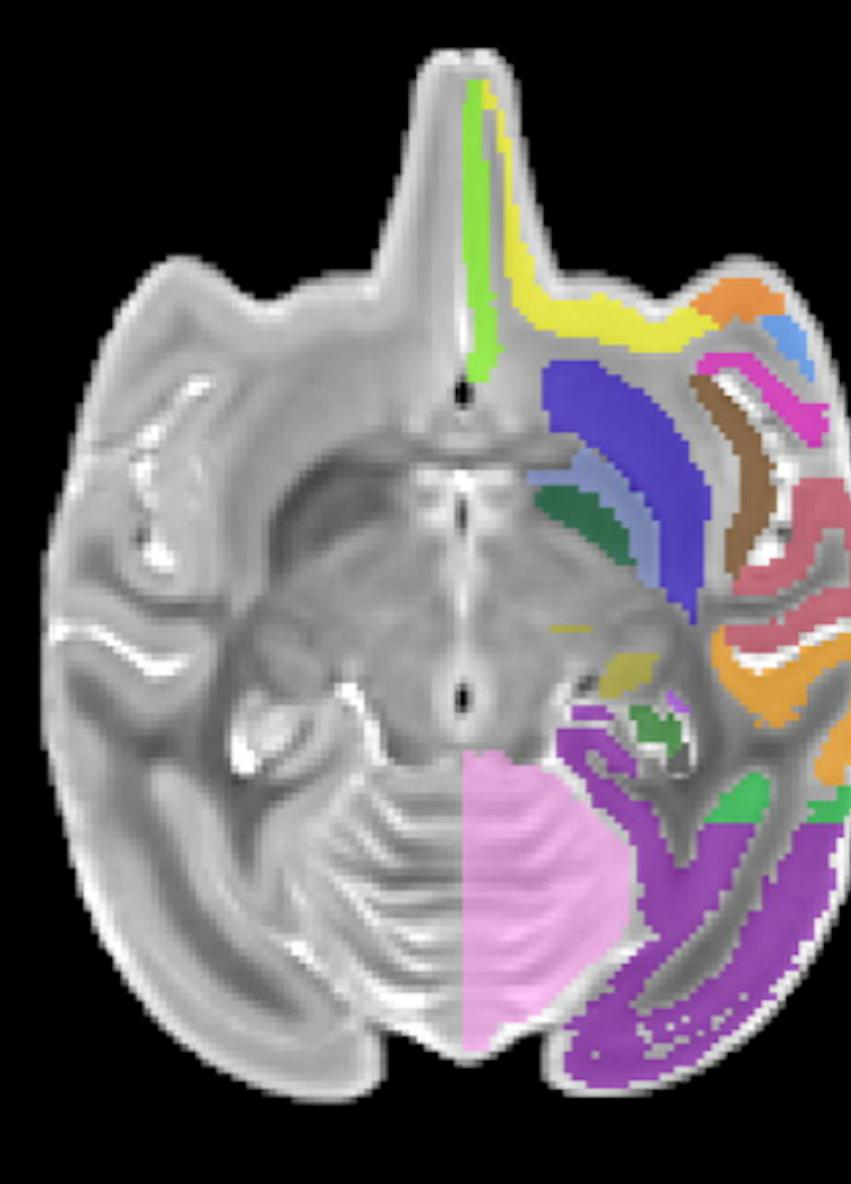


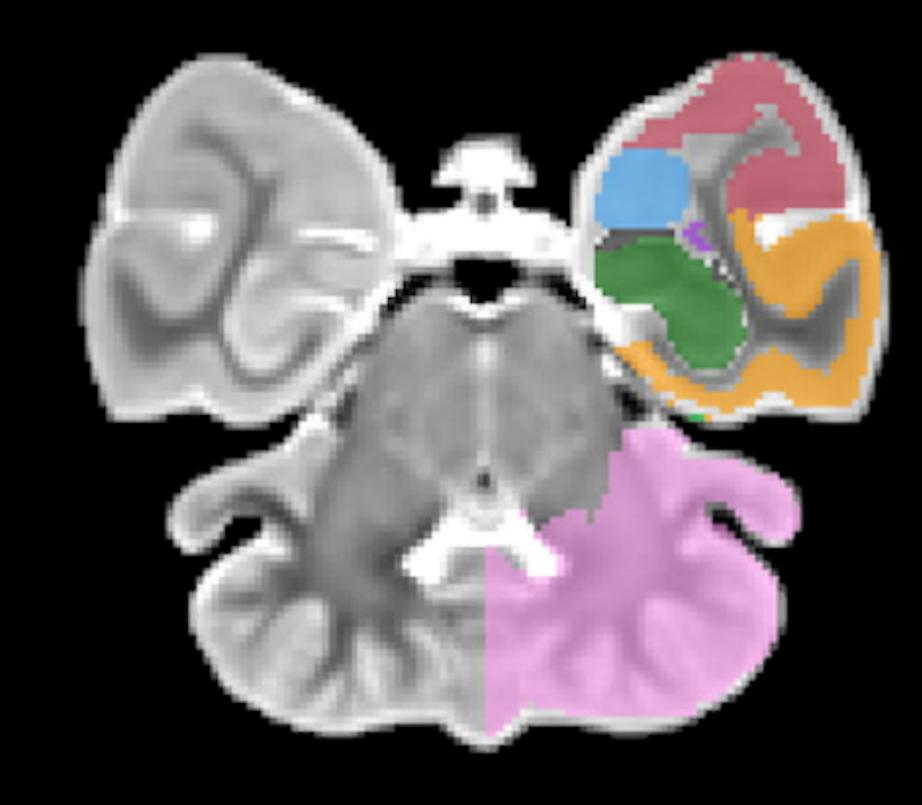






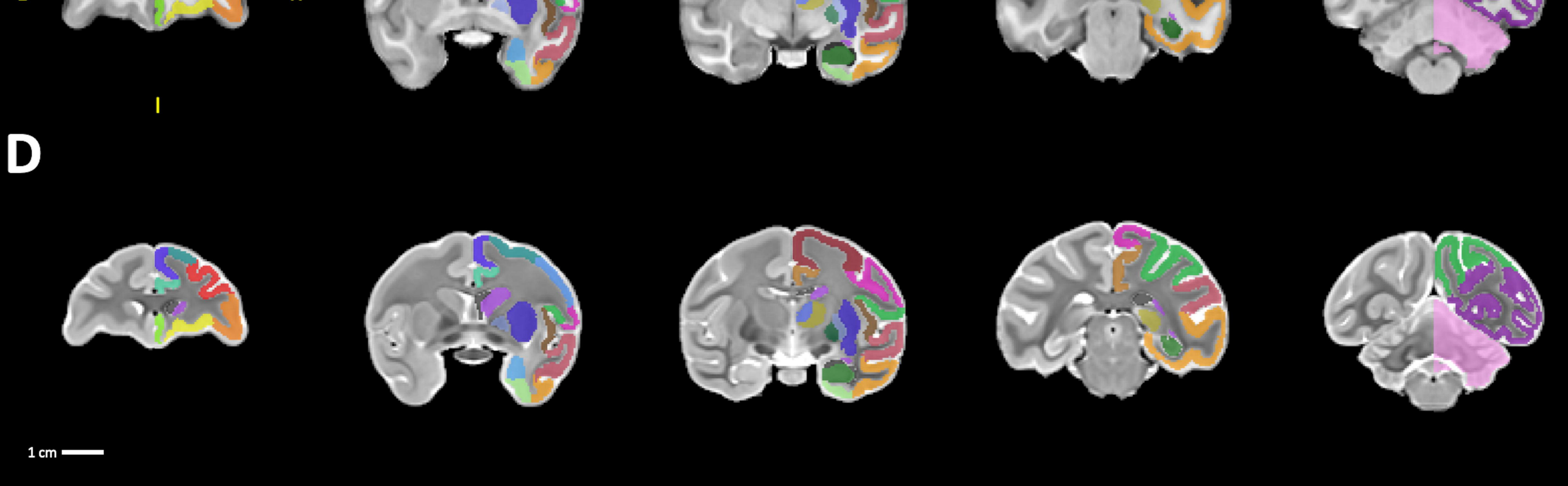






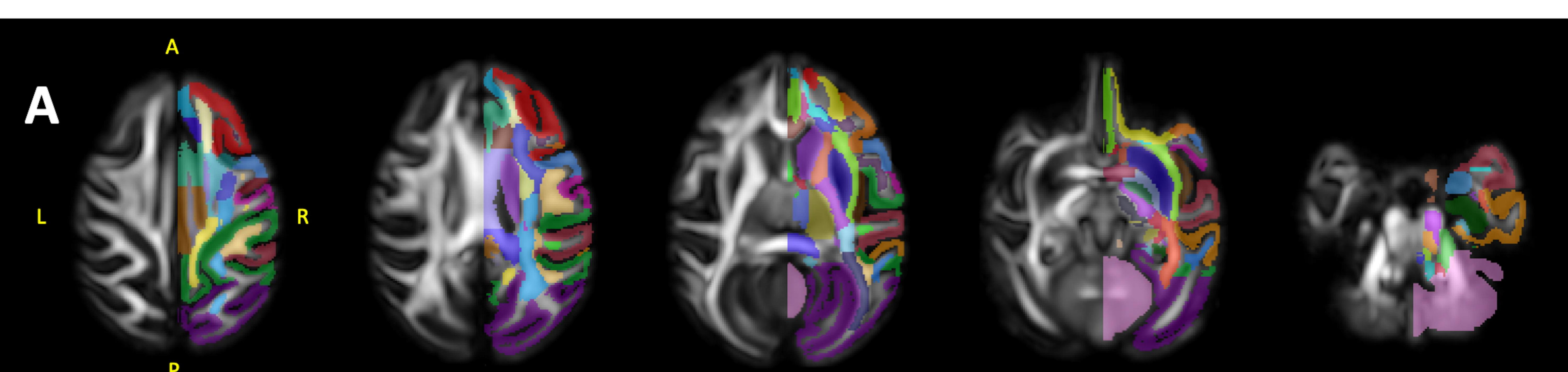




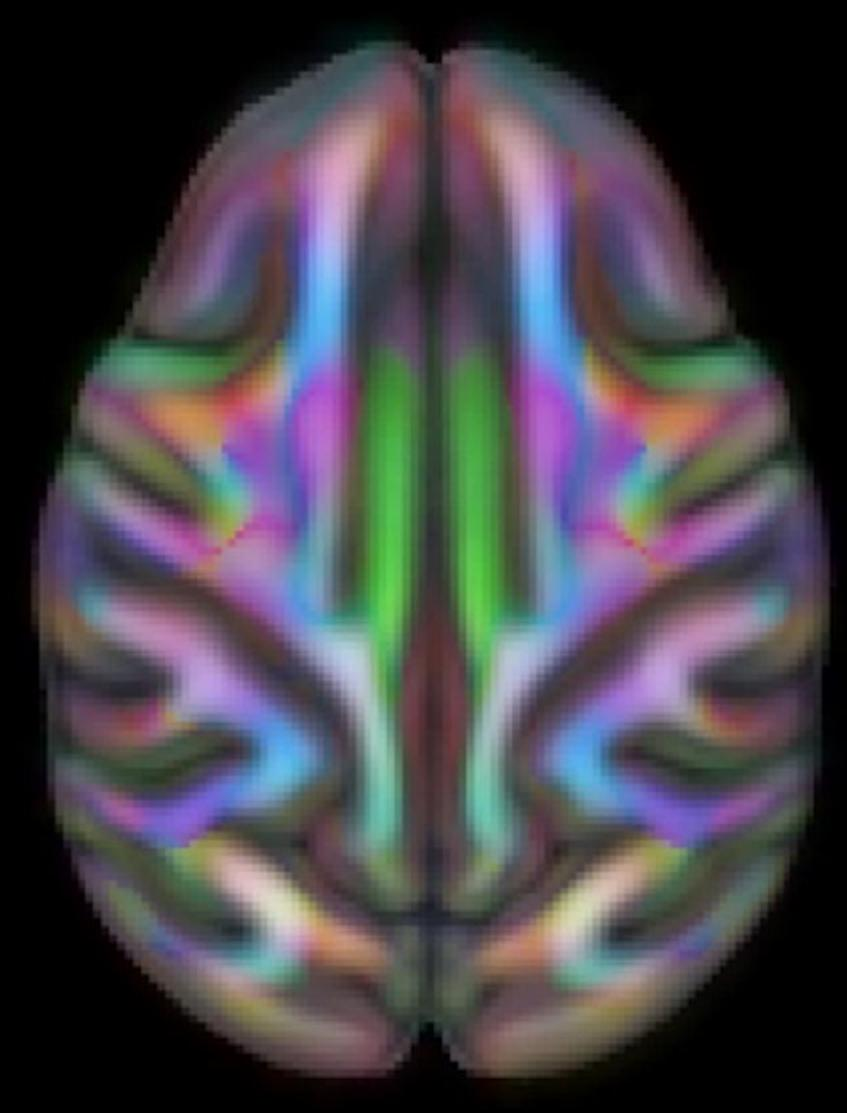


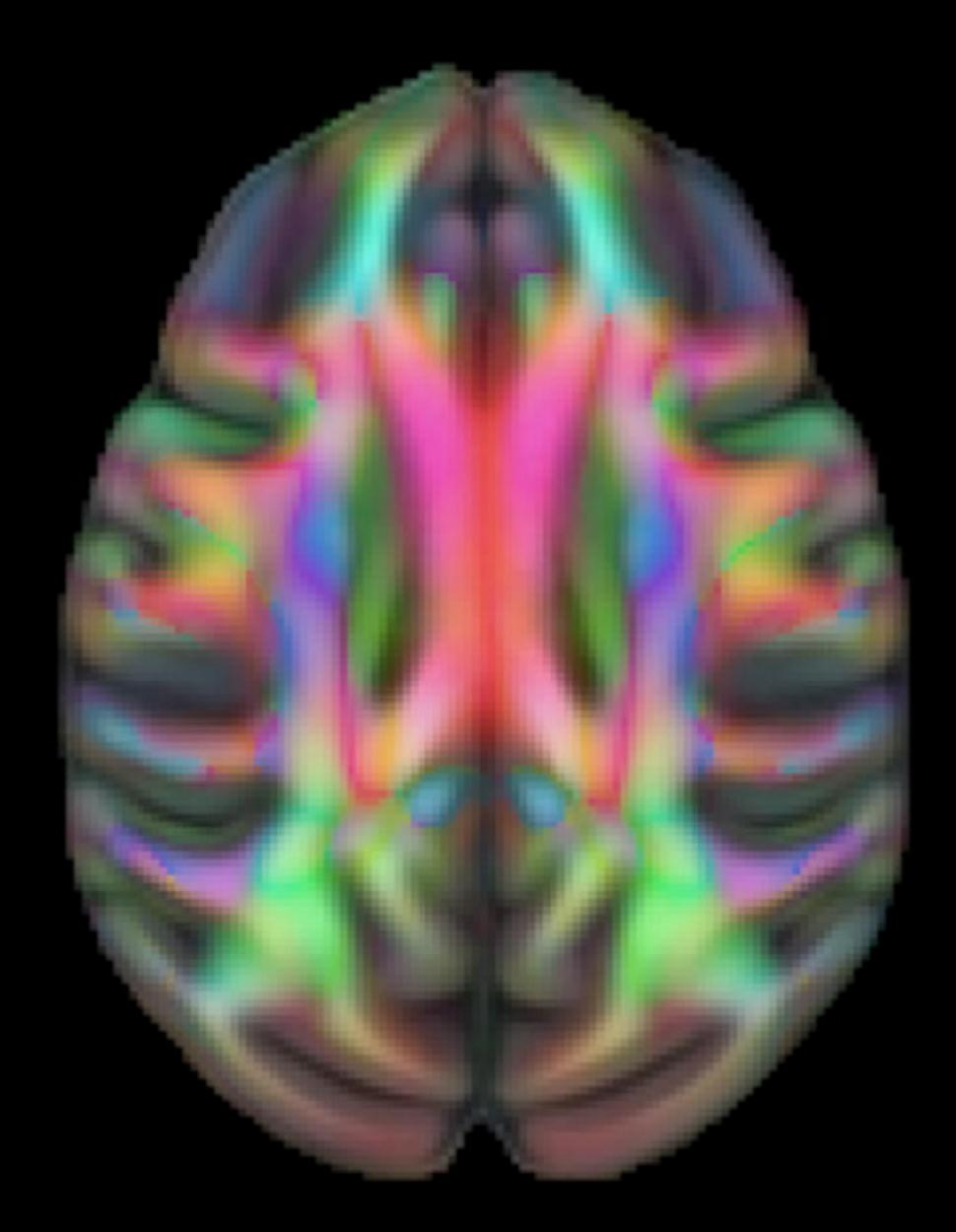
**Figure 2: sMRI templates.** A series of five axial and coronal sections displayed in neurological orientation through the T1 templates (A, C) and the T2 templates (B, D). For ease of viewing, the labelmap overlays are drawn only on the right hemisphere. *Abbreviations: A, anterior; I, inferior; L, left; P, posterior; R, right; S, superior.* 

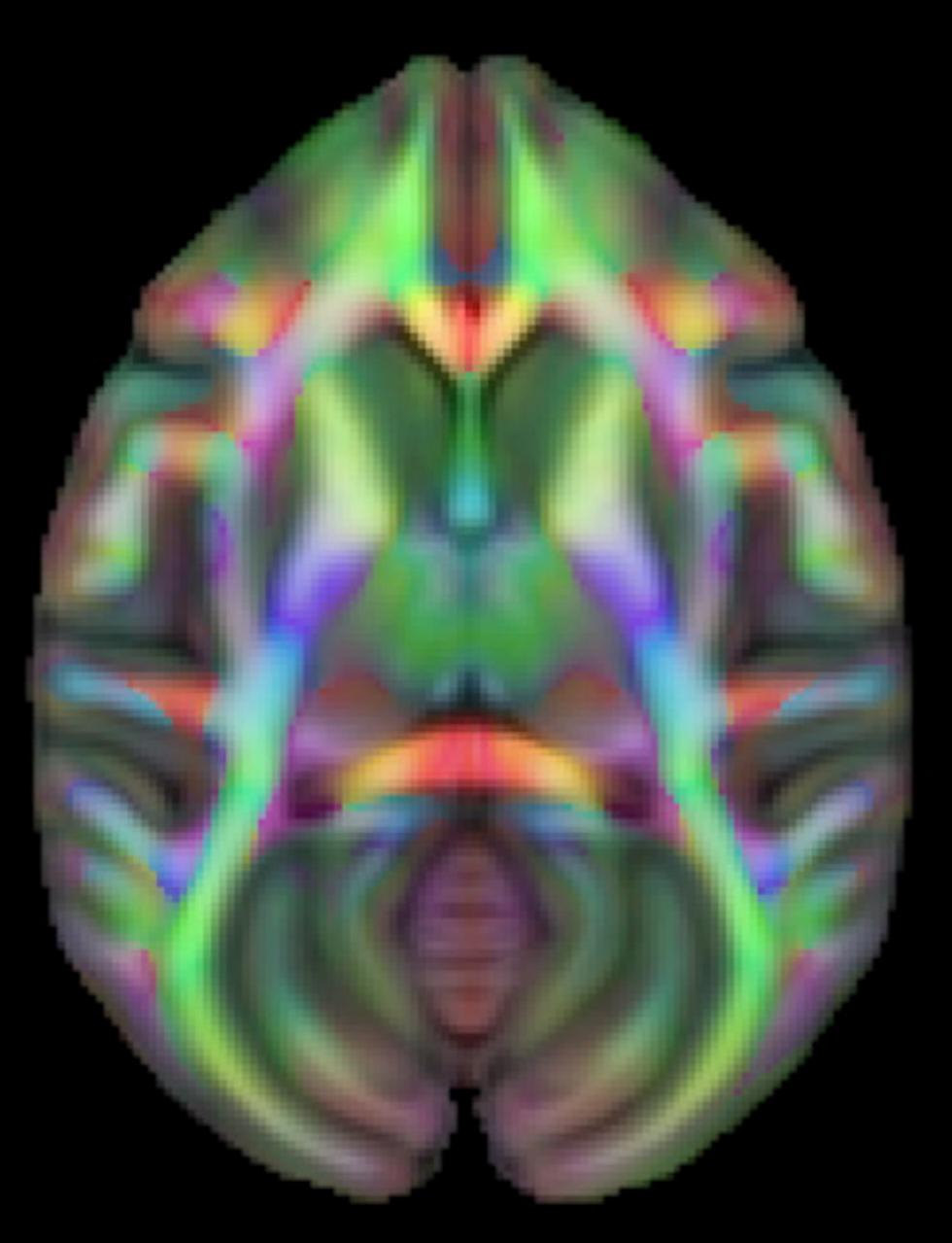
Figure 3.

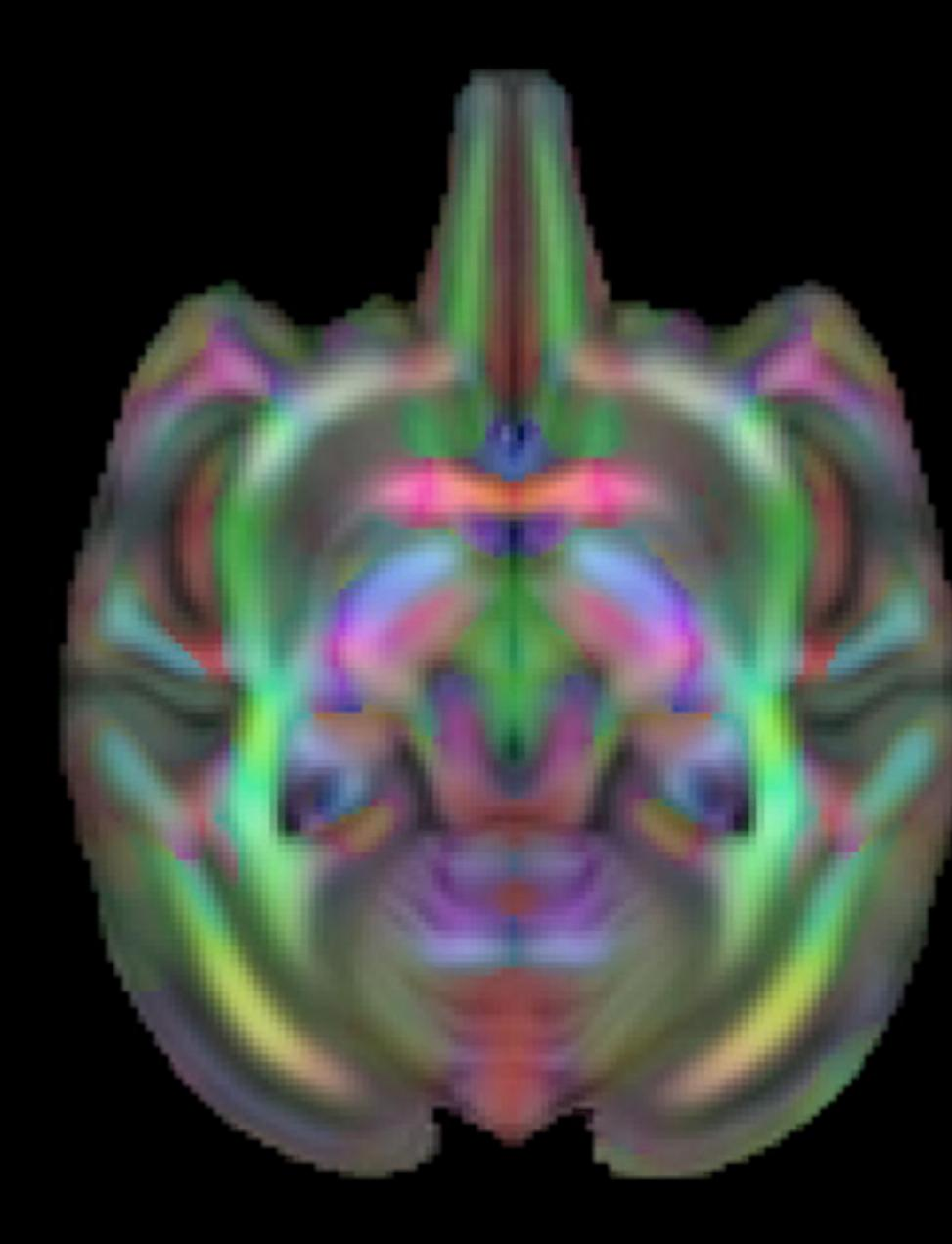


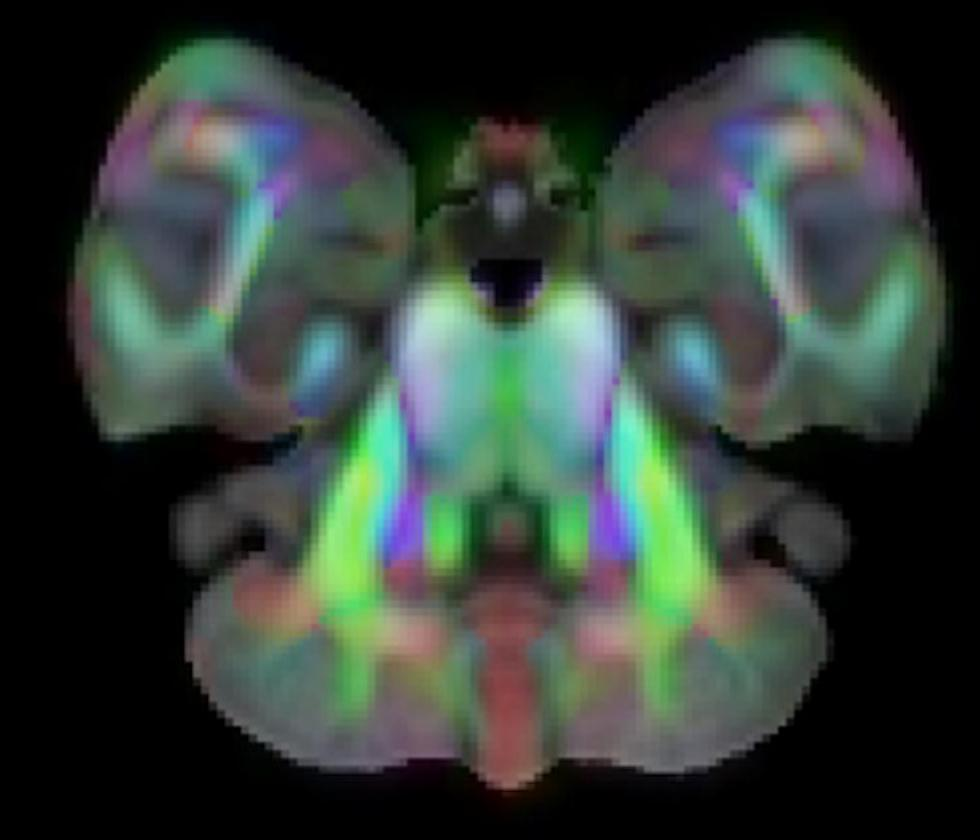




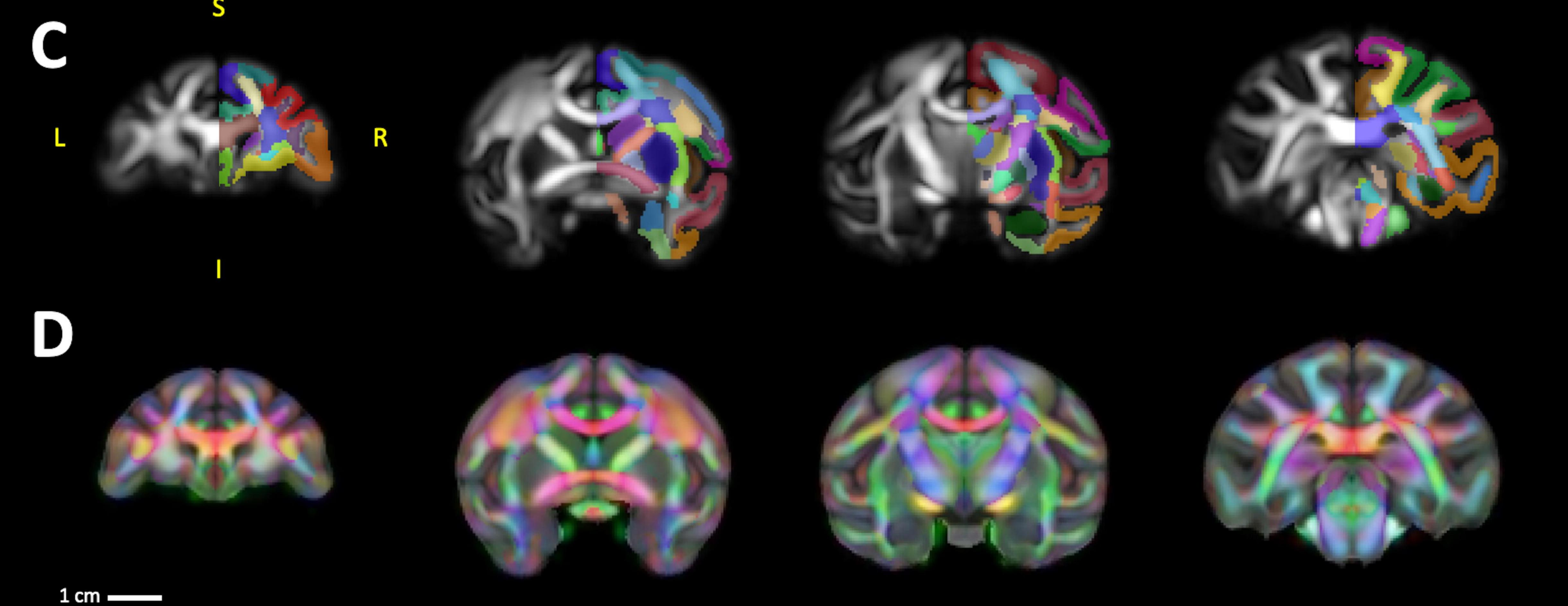


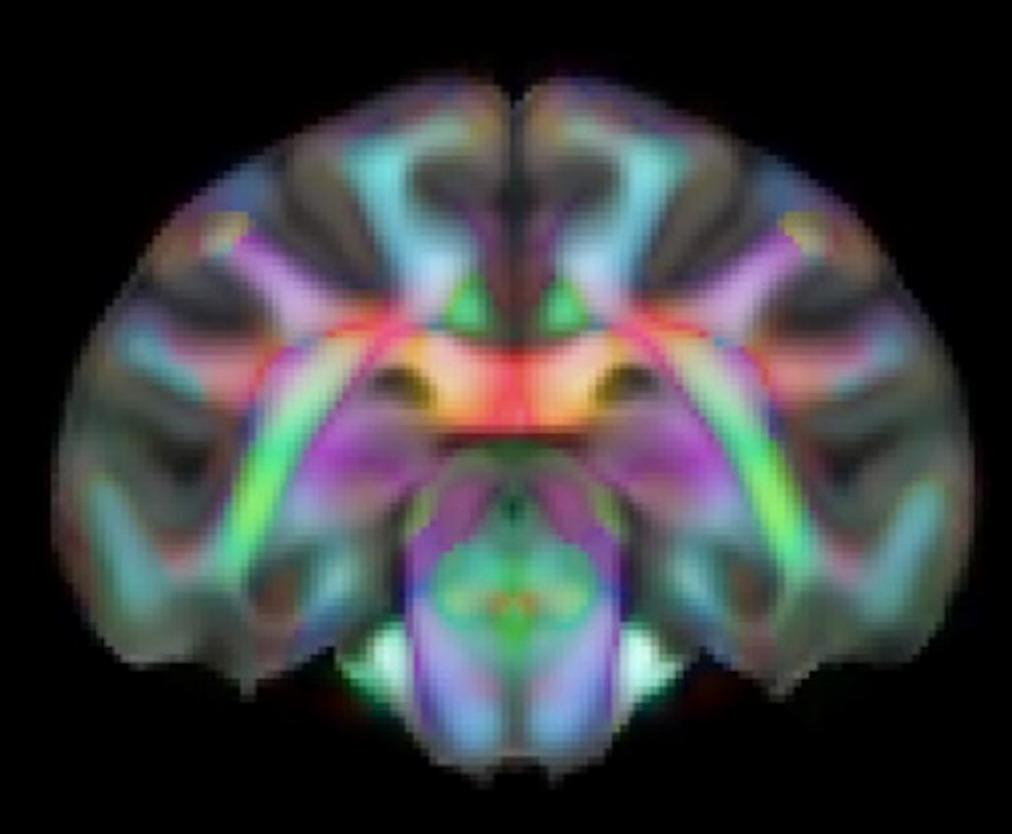


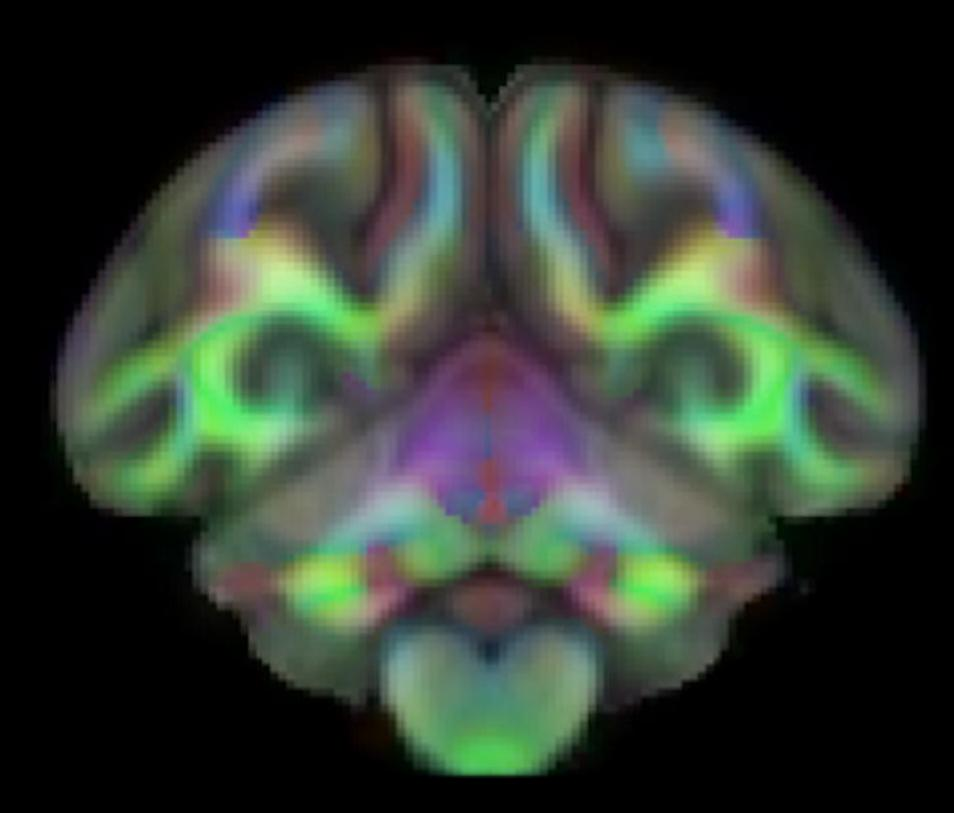












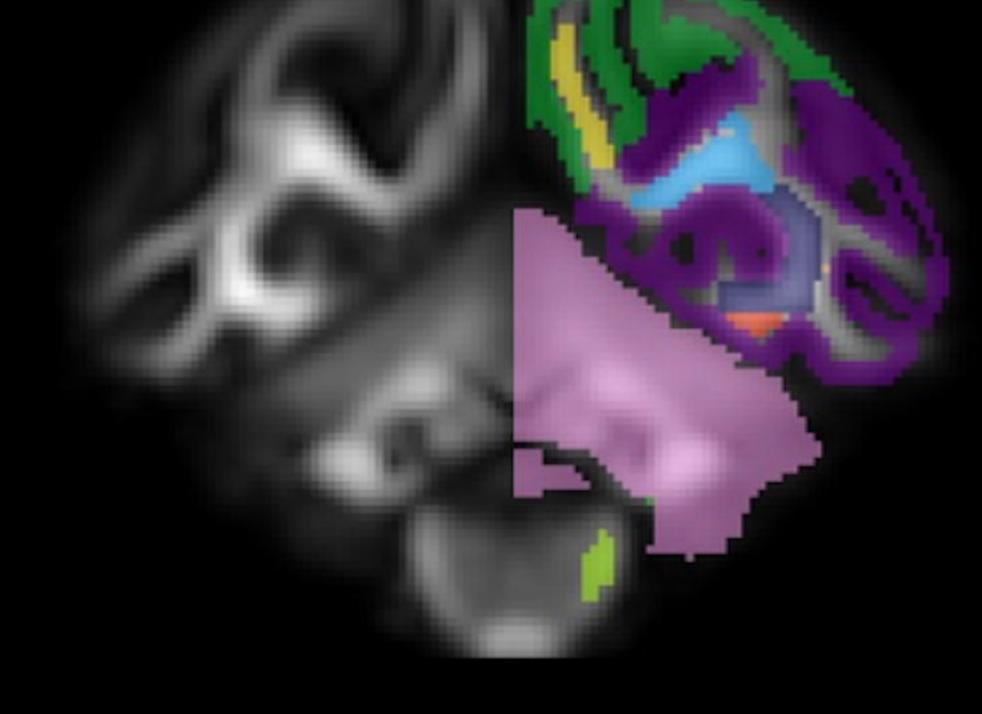
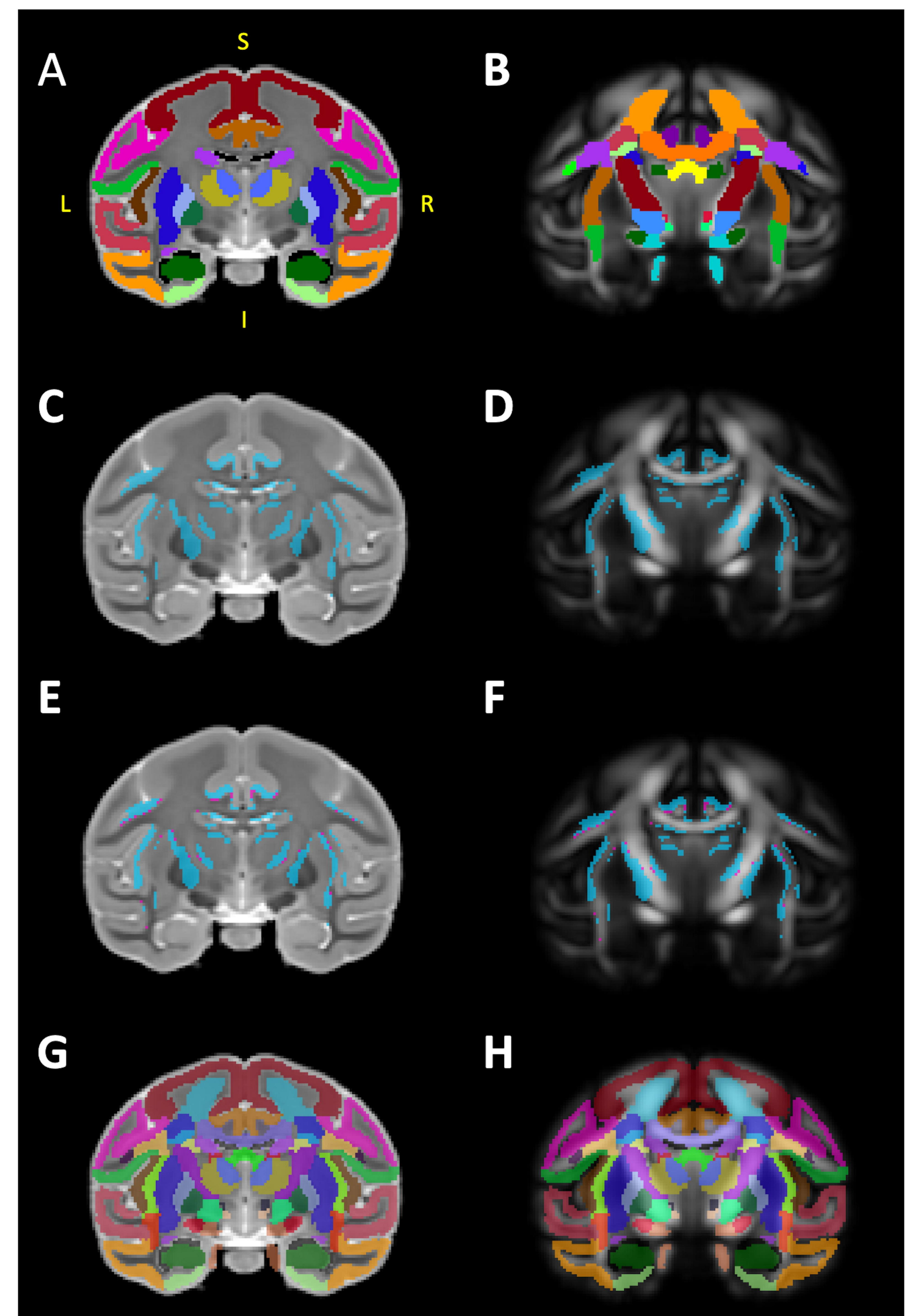


Figure 3: DTI Templates. A series of five axial and coronal sections displayed in neurological orientation through the FA template (A, C). For ease of viewing, the labelmap overlays are drawn only on the right hemisphere of the FA templates. To highlight the spatial co-registration of the DTI template with the sMRI templates (B, D) show visualization of RGB template as an overlay on the T1w template. Abbreviations: A, anterior; I, inferior; L, left; P, posterior; R, right; S, superior.





**Figure 4: Combing gray and white matter labelmaps.** (A) illustrates our gray matter (GM) labelmap overlaying the T2 template. We used a published diffusion tensor-based rhesus macaque atlas (Zakszewski et al., 2014) to identify and segment white matter tracts on our FA template, illustrated in (B). In order to combine these two labelmaps, using FSL tools, we first identified overlaps (i.e. double-labeled voxels) between the WM labelmap and our GM labelmap, these voxels are illustrated in blue in (C) and (D). ITK-SNAP was used to manually categorize these voxels as belonging to WM or GM, and the results of this classification is illustrated in (E) and (F), with blue voxels categorized as GM and magenta voxels categorized as WM. Finally, the categorized voxels were re-assigned to the appropriate GM/WM labelmap and ROI, and the two labelmaps were then consolidated into one. The results of this combination are illustrated in (G) and (H), overlaying the T2 and FA templates. *Abbreviations: I, inferior; L, left; P, posterior; R, right.* 

### Figure 5

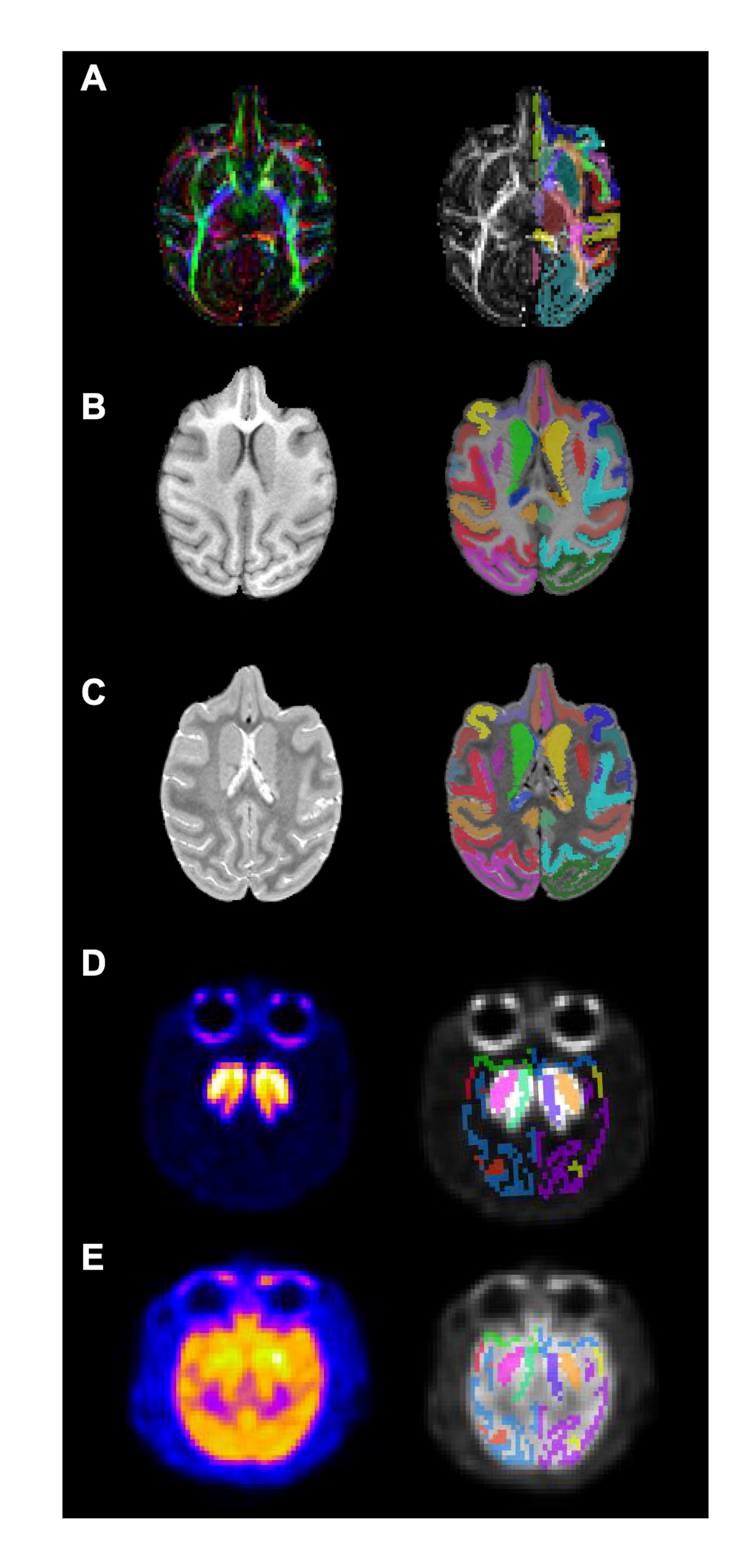


**Figure 5: Example application of multimodal templates.** A series of axial sections with co-registered labelmaps that illustrate several applications to scans collected from individual macaques using a variety of neuroimaging contrasts and modalities (DTI, sMRI, PET). Label maps were generated by AntsRegistration software version 2.1; (<u>http://stnava.github.io/ANTs/</u>). (A) DTI scan acquired from one of the individuals in the template at a later timepoint. (B, C) sMRI scans (T1w/T2w) that were collected from a juvenile (3yo) Japanese macaque (Macaca fuscata). (D, E) 18F-Fallypride PET and 18F-FDG PET in a naïve female rhesus macaque. These examples demonstrate some of the potential applications for this atlas, and suggest that it can be a reliable and versatile tool for a wide variety of different kinds of macaque neuroimaging studies.